NUCLEAR DESIGN OF THE BLANKET/SHIELD SYSTEM FOR A TOKAMAK EXPERIMENTAL POWER REACTOR

REACTORS

KEYWORDS: *shielding, breeding blankets, Tokamak devices, size, design, cost, neutron reactions, superconducting magnets, physical radiation effects, wall loading*

MOHAMED A. ABDOU *Argonne National Laboratory, Applied Physics Division*
9700 S. Cass Ave., Argonne, Illinois 60439

Received August 4, 1975
Accepted for Publication October 3, 1975

The various options and trade-offs in the nuclear design of the blanket/shield for a Tokamak Experimental Power Reactor (TEPR) are investigated. The TEPR size and cost are particularly sensitive to the blanket/shield thickness, Δ_{BS}, on the inner side of the torus. Radiation damage to the components of the superconducting magnet and refrigeration power requirements set lower limits on Δ_{BS}. These limits are developed in terms of TEPR design parameters such as the wall loading, duty cycle, and frequency of magnet anneals. The study of the nuclear performance of various material compositions shows that mixtures of tungsten, or tantalum, or stainless-steel alloys and boron carbide require the smallest Δ_{BS} for a given attenuation. This Δ_{BS} has to be doubled if the low induced activation materials graphite and aluminum are used. The space problems are greatly eased in the Argonne National Laboratory ANL-TEPR reference design by using two separate segments of the blanket/shield. The inner segment occupies the region of the high magnetic field, uses very efficient attenuators (tungsten- or tantalum- or stainless-steel-boron carbide mixtures), and is only 1 m thick. The outer blanket/shield is 131 cm and consists of an optimized composition of stainless steel and boron carbide. For the design parameters of 0.2 MW/m^2 neutron wall loading and 50% duty cycle, the reactor components can operate satisfactorily up to (a) 10 yr for the stainless-steel first wall, (b) 10 yr for the superconductor composite after which magnet warmup becomes necessary, and (c) 30 yr for the Mylar insulation. Nuclear heat generation rates in the blanket/shield and magnet are well within the practical limits for heat removal.

I. INTRODUCTION

Controlled thermonuclear research for Tokamaks has accomplished substantial progress in recent years.[1] The Tokamak Fusion Test Reactor[2] (TFTR), to be operational in ~1980 in Princeton, is planned to operate in a reactor regime D-T plasma and demonstrate plasma energy breakeven conditions. The next step beyond TFTR is the construction of a Tokamak Experimental Power Reactor (TEPR), which demonstrates the technological feasibility of a power producing Tokamak. The first TEPR is projected to operate as early as 1985 and produce tens of megawatts of electrical power.[3] Conceptual design studies have recently been undertaken by groups at Argonne National Laboratory[4-6] (ANL), General Atomic[7,8] (GA), and Oak Ridge National Laboratory[9,10] (ORNL). The purpose of this paper is to investigate the important aspects of the nuclear design for the TEPR blanket/shield system.

Since the TEPR will operate on the D-T cycle, 17.6 MeV of energy is released per fusion reaction in the form of an alpha particle and a neutron with average kinetic energies of 3.5 and 14.1 MeV, respectively. These average energies and the neutron spectra will be affected to some extent by the energies of the neutrals injected into the plasma as well as the plasma-ion temperatures, but the effects are small as far as the analysis in this paper is concerned. The 14-MeV neutrons represent the main source of recoverable energy in a D-T fueled fusion reactor, and they must be exploited in an energy conversion system with provision for sensible heat removal. Regardless of whether the reactor is designed to produce electrical power or just to demonstrate the feasibility of doing so, sufficient shielding must be provided against these neutrons to protect the toroidal field magnet and other reactor components. The toroidal-field coils for TEPR must

be superconducting since power losses in ordinary water-cooled copper coils would be too large to realize net power output. The choice of a superconducting magnet to produce the toroidal magnetic field in TEPR imposes a set of stringent requirements on the design of the blanket/shield system.

The space between the plasma region and the toroidal-field coils is generally considered as two separate regions, the blanket and the magnet shield. The blanket is the region in which most (~99%) of the kinetic energy of the neutrons and the resulting secondary gamma rays is converted into heat. The blanket is operated at reasonably high temperature to obtain an adequate thermodynamic efficiency in the case of an electrical power producing device and to keep cooling requirements to a manageable level in the case of no electrical power production. If tritium breeding is a design objective, a zone of lithium in one form or another must be provided in the blanket region. The energy conversion requirements are generally satisfied by blankets that give roughly two orders of magnitude attenuation in nuclear radiation. However, the superconducting magnet, which is cryogenically cooled to ~4 K, requires, as is shown later, another four orders of magnitude attenuation of the neutrons and photons streaming out of the blanket. This attenuation is provided by the magnet shield.

The primary functions of the magnet shield are:

1. To reduce the nuclear heating in the magnet to the levels allowed by (a) total power required to run the refrigerators and (b) the maximum local heat-generation rates imposed by practical limits for coil design (e.g., maximum allowable temperature increase in superconductor and normal conductor, heat transfer area, and spacing between coolant channels, etc.).

2. To attenuate the nuclear radiation to the minimum allowed by tolerable radiation damage to the components of the superconducting magnet. These components are (a) the superconductor, (b) the normal (stabilizing) conductor, (c) structural materials, (d) electrical insulators, and (e) thermal superinsulators. Of particular concern in examining the radiation damage effects in the magnet components is the reduction in the critical current density, J_c, in the superconductor and the increase in the resistivity of the normal conductor.

3. To reduce the level of radioactivity in the magnet to a tolerable level. Reliable performance of the superconducting magnet is of extreme importance for satisfactory operation of TEPR. This stringent requirement of reliability may dictate the construction of a permanent superconducting magnet, i.e., a magnet that would not be disassembled except under extreme circumstances. In this case, magnet maintenance has to be performed in place; it is, therefore, desirable to minimize the radiation-induced activation in the magnet components so that magnet maintenance and minor repairs can be made in place with a minimal degree of radiation protection after a reasonably short cool-down time. As is shown later, it is imperative that the reactor be shut down prior to any maintenance or repair work on components within the nuclear island.

Depending on design characteristics such as power level and blanket/shield material composition, satisfying the above requirements may be possible only with a relatively thick blanket/shield. On the other hand, increasing the blanket/shield thickness, Δ_{BS}, reduces the reactor power and increases the reactor cost. The reactor thermal power, P_T, can be written as

$$P_T = C\left(\frac{B_t}{A}\right)^4 Ra^2 \quad , \tag{1}$$

where

a = plasma minor radius

R = plasma major radius

A = aspect ratio = R/a

B_t = toroidal magnetic field at the plasma centerline

$$B_t = \left(1 - \frac{r_w + \Delta_{BS}}{R}\right) B_{\max} \tag{2}$$

r_w = first wall radius

$B_{\max}$ = maximum toroidal magnetic field at the inner coil winding.

The term C is a parameter that depends on other variables of no concern here. Selection of a particular superconducting material, such as NbTi, sets a practical upper limit on $B_{\max}$. Equations (1) and (2) show that, for fixed minor and major radii, B_t and P_T decrease as Δ_{BS} is increased. In addition, increasing the inner radius ($r_w + \Delta_{BS}$) of the magnet increases its cost. Equation (2) also shows that for fixed $B_t/B_{\max}$, the maximum allowable Δ_{BS} is smaller for reactors with smaller major radius. Considerations of low cost and significant electrical power production indicate[4] that, for reasonable assumptions about plasma confinement, TEPR will probably have $R \approx 5$ to 7 m for circular and ~4 to 6 m for noncircular plasma cross sections. This restricts the allowable space for the TEPR blanket/shield and makes its design

more difficult than that for large full-scale devices ($R \approx 10$ to 15 m).

It is clear from the above discussion that a prudent design for TEPR must include careful and in-depth analyses of the blanket/shield system. The various options and trade-offs in the nuclear design of this system are examined in detail in this paper. In Sec. II, we examine the nuclear performance of various material compositions for both the blanket and magnet shield. Section III is devoted to a study of the important considerations for selection of dimensions for the blanket and magnet shield. Quantitative magnet protection criteria are also developed in this section. Detailed description and analyses of a complete conceptual design are given in Sec. IV. Finally, the conclusions of this study are presented in Sec. V.

II. NUCLEAR PERFORMANCE OF VARIOUS MATERIAL COMPOSITIONS

Nuclear performance of materials is one of the most important aspects to be considered in the selection of material composition for the blanket and magnet shield. The effectiveness of various materials in attenuating neutrons and secondary gamma rays is investigated and compared in this section.

Selection of material composition for the blanket/shield depends on several other considerations besides effectiveness in neutron and gamma-ray attenuation. Material properties such as melting points, useful operating temperature ranges, material behavior under irradiation, compatibility with other system components (e.g., the coolant), and cost are some of these important considerations. Furthermore, material selection for the blanket and magnet shield depends to a large degree on the major requirements of and constraints on the overall reactor design. For example, if tritium breeding is required, then lithium in one form or another must be used in the blanket.

The high energy of the D-T neutron imposes a particularly difficult shielding problem in fusion devices operated on the D-T cycle. Space restrictions are particularly severe in small-size reactors and are further complicated by the necessity of using a NbTi superconductor in which the maximum practical magnetic field is limited to ~80 kg. A basic requirement, therefore, of materials to be used in the TEPR blanket/shield is to have large attenuation coefficients for high-energy neutrons and gamma rays. Materials satisfying these requirements are generally of moderate or large mass number (e.g., iron, lead, tantalum, and tungsten) because inelastic scattering is the most efficient mechanism for reducing the energies of the high-energy neutrons and because gamma-ray attenuation increases significantly with the atomic number. Below the inelastic threshold, however, the neutron attenuation effectiveness of these materials is greatly reduced, and a lighter element (e.g., water, polyethylene, lithium hydride, or graphite) should be present in the blanket/shield. Furthermore, to minimize the gamma-ray emission from radiative capture reactions, the use of an appropriate amount of a strong neutron absorber (e.g., boron) is necessary.

Three recent studies of fusion reactor magnet shielding have been reported in Refs. 11, 12, and 13. The study of Kriese and Steiner[11] examined the attenuation properties of several materials in the magnet shield coupled to a 1-m natural lithium-graphite blanket. Among the materials considered, they found that in terms of reducing the magnet heating in a fixed shield thickness a tantalum-borated graphite mixture was the most and borated graphite the least efficient with lithium hydride, borated water, and polyethylene in between. Abdou and Maynard[12] examined several possible shielding materials and made an attempt to optimize the magnet shield dimensions and composition on the basis of minimum reactor cost. Their study concentrated on large commercial reactors (major radius ~13 m) with lithium blankets. They concluded, for the materials investigated, that

1. A mixture of 70% stainless steel plus 30% boron carbide results in the smallest magnet shield thickness for a given tolerable level of nuclear heating in the magnet.
2. Although a mixture of 70% lead plus 30% boron carbide requires a much larger shield thickness than the 70% stainless steel plus 30% B_4C mixture, the former results in a lower overall cost.
3. The requirements of magnet protection are satisfied by the cost-optimized shield.
4. Optimum shield composition and dimensions are moderately sensitive to reactor wall radius, wall loading, material cost, refrigerator capital cost, as well as several other parameters.

The study did not cover the effect of varying the major radius on the optimization results. Gabriel et al.[13] investigated the shield design for the ORMAK-F/BX, the ORNL version of the TFTR, which has a plasma radius of 120 cm. They selected a shield that consists of a 35-cm-thick

region of 65% iron plus 35% borated water surrounded by a 5-cm-thick lead liner. They found that this shield is very adequate to protect the magnet at a peak fusion power of 6 MW for a total fusion energy generation of 4×10^7 MJ.

The possible options for a TEPR where the size, space restrictions, and objectives lie between the TFTR and large-scale commercial reactors are examined in this study. The nuclear performance of various materials is compared primarily on the basis of nuclear heating and radiation damage in the magnet. The total (neutron plus gamma-ray) energy leakage from the shield to the magnet is taken as a measure of energy deposition in the magnet. One of the most important effects of radiation damage to a cyrogenically stabilized magnet is the increase in the resistivity of the normal-conductor stabilizer. Here we select copper as the stabilizer and atomic displacement as the radiation damage indicator. The correlation between radiation-induced resistivity and atomic displacement is derived in the following section. Five sets of designs—A, B, C, D, and E—are examined. Each set consists of several alternative designs that cover the options for a particular concept of the TEPR blanket/shield. Since some of the designs are used in more than one set, each design is given a unique three-digit number. The description of dimensions and material compositions for the various designs in the five sets is given in Tables I through V. All percentages in material composition given in these tables, and everywhere else in this paper, are on a volume basis.

The neutron and gamma-ray fluxes were calculated in all cases by solving the discrete ordinates form of the transport equation using the ANISN (Ref. 14) program in the S_8-P_3 approximation in one-dimensional (1-D) cylindrical geometry. The 1-D calculations are used here only for the purpose of comparing the nuclear performance of various materials and examining the gross behavior of the blanket/shield. Detailed engineering design of a TEPR requires, of course, multidimensional neutronics and photonics calculations for accurate treatment of the toroidal geometry and penetrations such as vacuum and injector ports. In all calculations, 100 energy groups were used for the neutrons and 43 groups for the gamma rays. The neutron and gamma-ray multigroup cross sections were processed using SUPERTOG (Ref. 15) and MUG (Ref. 16). The photon production cross sections were processed with LAPHNGAS (Ref. 17). The neutron multigroup reaction cross sections and kerma factors were generated with MACK (Ref. 18). Nuclear data of ENDF/B-III (Ref. 19) were used in all cases. The displacement cross sections reported in Ref. 20 were used except in the case of copper which, for the purpose of this work, were generated with a displacement energy of 40 eV.

One of the design objectives for TEPR is to demonstrate the capability of tritium production, extraction, and processing. The effects of lithium

TABLE I

Description* of Design Set A

(Thickness and enrichment of lithium are varied.)

Design No.	Blanket	Reflector	Shield
101	25 cm 90% natural[a] lithium + 10% vanadium	5 cm SS	50% SS + 50% B_4C
102	25 cm Stainless steel	5 cm SS	50% SS + 50% B_4C
109	2 cm 90% enriched[b] lithium + 10% vanadium 5 cm 90% beryllium + 10% vanadium 3 cm 90% enriched[b] lithium + 10% vanadium 15 cm stainless steel	5 cm SS	50% SS + 50% B_4C
110	2 cm 90% enriched[b] lithium + 10% vanadium 5 cm stainless steel 3 cm 90% enriched lithium + 10% vanadium 15 cm stainless steel	5 cm SS	50% SS + 50% B_4C
111	35 cm 90% natural lithium + 10% vanadium	5 cm SS	50% SS + 50% B_4C

*All percentages in material composition are volume percentages.
[a]Isotopic composition of natural lithium is 7.42% ^6Li and 92.58% ^7Li.
[b]Enriched lithium of 90% ^6Li and 10% ^7Li isotopic composition.

thickness and enrichment on the amount of tritium produced and the total blanket/shield thickness Δ_{BS} are examined by design set A. The set consists of designs 101, 102, 109, 110, and 111 as shown in Table I. In all five designs, a 5-cm-thick reflector of stainless steel (SS) and a shield of variable thickness with a 50% stainless-steel plus 50% B_4C composition were used. The blankets in designs 101 and 111 are, respectively, 25- and 35-cm-thick zones containing 90% natural lithium plus 10% structure. Vanadium was used in the 1-cm-thick first wall and as the structural material. Results derived here are not overly sensitive to this choice. Design 102 uses a 25-cm-thick blanket of stainless steel. The blanket in design 109 consists of 2- and 3-cm regions of 90% enriched lithium plus 10% vanadium separated by a 5-cm zone of 90% beryllium plus 10% vanadium and followed in the outer region by 15-cm stainless steel. Design 110 is similar to design 109 except that the 5-cm beryllium-vanadium zone is replaced with stainless steel.

Tritium breeding ratios of 0.87, 1.1, 0.73, and 1.08 were calculated for designs 101, 109, 110, and 111, respectively. Figures 1 and 2 show the atomic displacement in units of dpa per (MW yr)/m^2 and the total energy leakage in units of MeV/D-T neutron, respectively, as a function of the blanket plus shield thickness Δ_{BS}. From considerations given in Sec. III, for a reasonable size TEPR [major radius, $R \approx 5$ to 7 m, thermal power $\approx$ 150 MW(th)], Δ_{BS} should be no more than

TABLE II

Description* of Design Set B

(Percentage of boron carbide in SS-B_4C mixture is varied.)

Design No.	Blanket	Reflector	Shield
101	25 cm 90% natural lithium + 10% vanadium	5 cm SS	50% SS + 50% B_4C
104	25 cm 90% natural lithium + 10% vanadium	5 cm SS	75% SS + 25% B_4C
105	25 cm 90% natural lithium + 10% vanadium	5 cm SS	25% SS + 75% B_4C
106	25 cm 90% natural lithium + 10% vanadium	5 cm SS	100% SS

*All percentages in material composition are volume percentages.

TABLE III

Description* of Design Set C

(Comparison of various coolants)

Design No.	Blanket	Reflector	Shield
101	25 cm 90% natural lithium + 10% vanadium	5 cm SS	50% SS + 50% B_4C
112	25 cm 90% natural lithium + 10% vanadium	5 cm SS	75% SS + 20% H_2O + 5% B
102	25 cm Stainless steel	5 cm SS	50% SS + 50% B_4C
116	25 cm Stainless steel	5 cm SS	75% SS + 20% H_2O + 5% B
120	30 cm 75% SS + 20% H_2O + 5% B		75% SS + 20% H_2O + 5% B

*All percentages in material composition are volume percentages.

TABLE IV

Description* of Design Set D

(Comparison of tungsten and stainless steel)

Design No.	Blanket	Shield
102	30 cm Stainless steel	50% SS + 50% B_4C
103	30 cm 50% SS + 50% B_4C	50% SS + 50% B_4C
108	30 cm 50% tungsten + 50% B_4C	50% tungsten + 50% B_4C

*All percentages in material composition are volume percentages.

1 m, the displacement rate in the stabilizer should be in the range of 10^{-4} to 10^{-3} dpa per (MW yr)/m^2, and the energy leakage to the magnet in the range of 10^{-5} to 10^{-3} MeV/D-T neutron. Note that the blanket plus shield thicknesses shown in all results for design sets A, B, C, D, and E do not include the space required for coolants, thermal expansion, access regions for fueling, dimensional changes due to radiation damage, etc. Thus, the actual blanket/shield thickness in the radial dimension from the first wall to the toroidal field coils will be ~15% larger than the values shown in this section. From results in Figs. 1 and 2 the following conclusions can be made:

1. Comparing the results for designs 101 and 111 shows that increasing T from 0.87 to 1.08 requires an increase in Δ_{BS} of ~6 cm.
2. The results for designs 109 (T = 1.1) and 111 (T = 1.08) show that using highly enriched lithium and beryllium instead of natural lithium could save as much as 20 cm on Δ_{BS}. In addition, using highly enriched lithium and beryllium instead of natural lithium makes it possible to minimize the lithium and tritium inventories as shown previously.[21]
3. Replacing beryllium in design 109 by stainless steel reduces T by ~35% and Δ_{BS} by only 2 cm.
4. Employing an all stainless-steel blanket in design 102 reduces Δ_{BS} by ~27 cm relative to the natural lithium blanket (design 111) but only by 5 cm relative to design 109 (^{6}Li-Be blanket).

Therefore, if tritium production with a high breeding ratio is required, there will be a penalty in terms of increasing Δ_{BS}, particularly if natural lithium is to be used as the breeding medium. The problem is greatly reduced by using highly enriched lithium (~90% ^{6}Li) in the presence of a neutron multiplier. Except for fissionable materials, beryllium is the best neutron multiplier. However, the magnitude of beryllium reserves and resources is not well known at present,[21] and it is uncertain whether beryllium can be used in relatively large quantities in commercial fusion reactors. Furthermore, since future fusion reactors are envisioned to be very large (major radius ≈ 10 to 15 m), the space restrictions on the size of the blanket/shield are much less complicated than in TEPR and, in this regard, tritium breeding with large quantities of natural lithium represents no serious problem. Thus, the use of beryllium in TEPR introduces a feature for the blanket that may not be extrapolatable to the Demonstration Reactor Plant[4] and future fusion reactors.

TABLE V

Description* of Design Set E

(Performance of low induced activation materials in the blanket and shield compared with other materials)

Design No.	Blanket	Shield
102	30 cm Stainless steel	50% SS + 50% B_4C
108	30 cm 50% tungsten + 50% B_4C	50% tungsten + 50% B_4C
113	30 cm Aluminum	50% SS + 50% B_4C
114	30 cm Aluminum	50% Al + 50% B_4C
117	30 cm Graphite	50% SS + 50% B_4C
118	30 cm Graphite	50% Al + 50% B_4C
119	30 cm Vanadium	50% SS + 50% B_4C

*All percentages in material composition are volume percentages.

Tritium production and extraction concurrently with energy conversion and heat removal will compound the difficulties of achieving the primary objectives of a TEPR. It is conceivable, therefore, that a TEPR could best be operated in at least two stages.[4] In Stage I, devoted to verification of plasma characteristics and power production aspects, there will be no lithium in the blanket. In Stage II, attention will be given to other aspects of a full-scale Tokamak reactor. In this later stage, experimentation with tritium production and extraction can be made. This can be accomplished by integrating one or more modules of lithium, or alternative lithium compound, into the blanket. Depending on the availability and cost of tritium supply for the TEPR

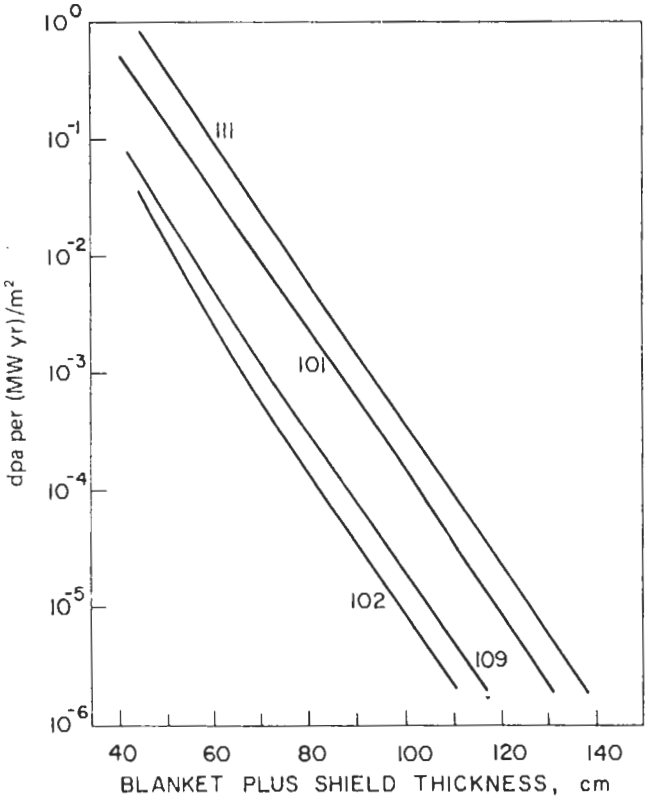

Fig. 1. Variation of atomic displacement in the magnet stabilizer (copper) with blanket plus shield thickness for designs in Set A.

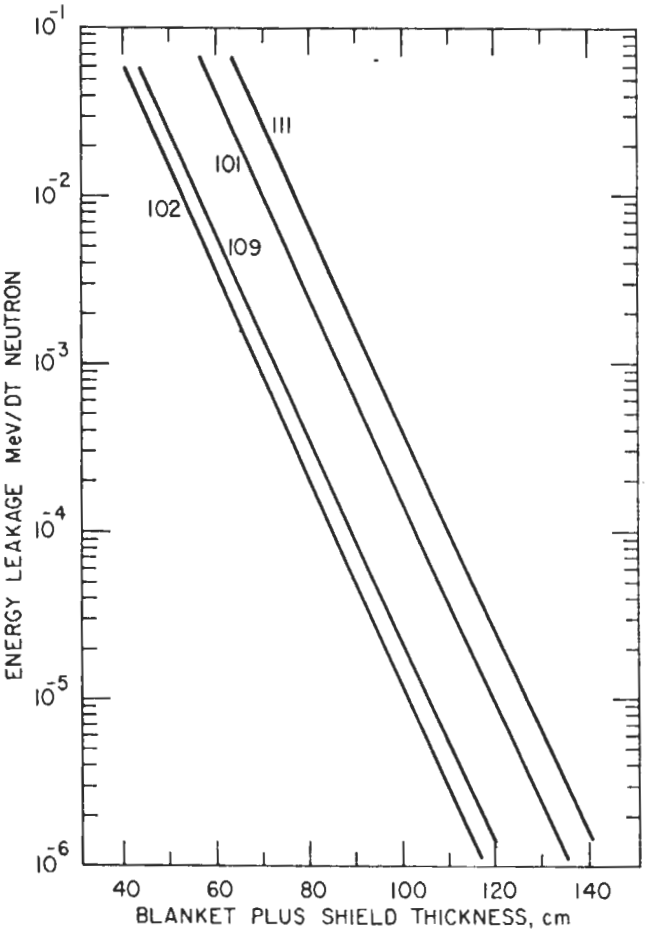

Fig. 2. Variation of total (neutron plus gamma-ray) energy leakage to the magnet with the blanket plus shield thickness for designs in Set A.

fuel, the entire blanket may have to be replaced in Stage II by a new one capable of yielding an overall tritium breeding ratio near unity. For the staged operation approach, the above results indicate a number of ways that experimental modules for Stage II could be designed to demonstrate tritium breeding capability. Alternative breeding materials, such as solid lithium compounds, are not examined here since they were investigated in great detail earlier.[21]

The optimum volume percentage of boron carbide (B_4C) in a stainless-steel B_4C shielding mixture is examined by design set B described in Table II. The set consists of designs 101, 104, 105, and 106. All of the four designs, which are possible Stage II modules, have a 1-cm vanadium first wall, 25-cm blanket of 90% natural lithium plus 10% vanadium, and a 5-cm stainless-steel reflector. The percentage of B_4C in the stainless-steel B_4C shield mixture is varied from zero in design 106, to 25% in design 104, to 50% in design 101, and to 75% in design 105. The variation of the atomic displacement in the magnet copper and the energy leakage to the magnet with the blanket-shield thickness are shown in Figs. 3 and 4, respectively. The results in Fig. 4 show that for a specified level of energy leakage to the magnet, Δ_{BS} is smallest for the 75% stainless steel plus 25% B_4C mixture, which is in agreement with the results of Ref. 12. However, in terms of copper displacement, Δ_{BS} is smallest for the 50% stainless steel plus 50% B_4C mixture. The difference in Δ_{BS} for the optimum compositions for atomic displacement and energy leakage is relatively small, but the reason why there is a difference is interesting. The energy leakage in the multigroup treatment is the sum over all groups of the neutron and gamma-ray current for each energy group multiplied by the effective energy for the group. The atomic displacement rate is the sum over all groups of the neutron flux for each group multiplied by the displacement cross section for this group. The displacement cross section for copper does not drop linearly with decreasing energy, e.g., its value at 1 MeV is ~25% of that at 10 MeV. Since a large fraction of the neutrons in the shield are shifted toward the

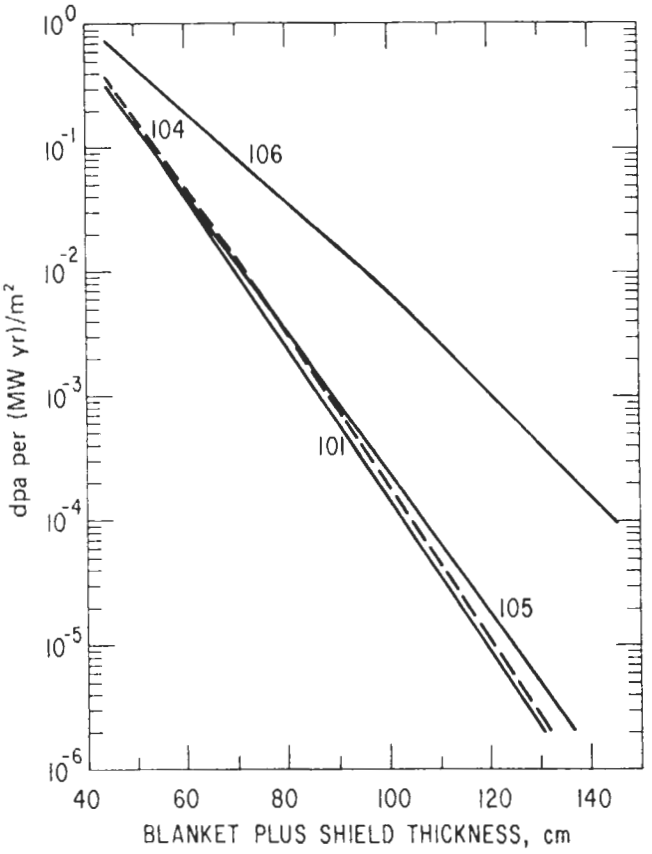

Fig. 3. Variation of atomic displacement in the magnet stabilizer (copper) with blanket plus shield thickness for designs in Set B.

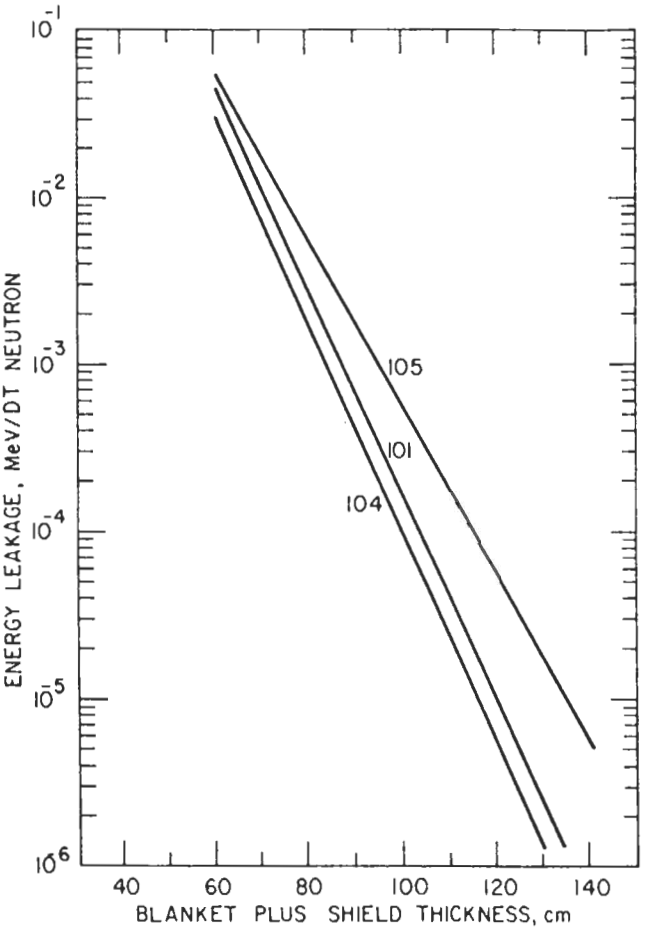

Fig. 4. Variation of total (neutron plus gamma-ray) energy leakage to the magnet with blanket plus shield thickness for designs in Set B.

low end of the MeV energy range, effective reduction of the atomic displacement in the magnet requires the use of a shield that has a large attenuation coefficient for low and intermediate energy neutrons, i.e., increasing the percentage of boron carbide. The energy leakage indicator, however, emphasizes the high energy range and includes the contribution from secondary gamma rays, thus favoring a higher percentage of stainless steel. However, using an all stainless-steel shield increases, for the same Δ_{BS}, the energy leakage and atomic displacement in the magnet by about two orders of magnitude relative to the other stainless-steel B_4C shield mixtures. This is because of the rapid buildup of neutrons in the keV and low MeV energy range and the significant increase in gamma-ray production from radiative capture reactions in stainless steel when B_4C is absent.

The two most likely candidates for TEPR coolant are helium and water. Lithium cooling in TEPR is a possibility for a Stage II module, providing that the necessary technology for handling liquid-metal coolants under the effect of strong magnetic fields is developed in a time period that meets the proposed schedule for TEPR. The use of water in the first stage with no lithium in the blanket may be possible if no melting of any part of the blanket/shield metallic components could be assured. However, when lithium in liquid or solid compound form is utilized in Stage II, water cooling is undesirable.

Neutronics effects of using water as a coolant and moderator compared with helium and lithium cooling are brought out by comparing the nuclear performance of designs 101, 112, 102, 116, and 120 in design set C (see Table III). Both designs 101 and 112 include a 25-cm-thick blanket of 90% natural lithium plus 10% vanadium. The lithium in both designs serves as the breeder and coolant in the blanket region and yields a tritium breeding ratio of ~0.9. The shield in design 101 is 50% stainless steel plus 50% B_4C and is helium cooled. The water-cooled shield in design 112 consists of 75% SS + 20% H_2O + 5% B. No internal cooling of

the 5-cm stainless-steel reflector is provided for as face cooling from the blanket and shield sides is adequate. Designs 102 and 116 compare the helium and water cooling of the shield as designs 101 and 112 do, but the blanket in each of these two designs is a helium-cooled 25-cm stainless-steel blanket. Design 120 is water cooled in the blanket, reflector, and shield, and consists of 75% SS + 20% H_2O + 5% B. The case of lithium cooling in the shield was not considered, since the heat generation rates in the shield are too low and it is advantageous to keep the shield at low operating temperature with no tritium contamination. Cooling the blanket with liquid lithium is a reasonable option only if tritium breeding is required.

Figures 5 and 6 show the atomic displacement in the magnet copper and the energy leakage to the magnet as functions of the blanket plus shield thickness for designs in set C. Since helium does not perturb the neutronics to any measurable extent, it was not included in the calculations. Helium affects the required blanket and shield thickness, however, through a void fraction that represents the ratio of the volume of the helium coolant to the blanket or shield material volume. From heat transfer considerations, an average void fraction of 10% in the blanket region and 5% in the shield region is adequate for proper cooling at a neutron wall loading of ~0.2 to 0.5 MW/m^2. Therefore, the blanket and shield thicknesses shown in Figs. 5 and 6 should be increased by 10 and 5%, respectively, in case of helium cooling. The amounts of water and lithium included in the calculations are more than sufficient for cooling purposes. (The 75% stainless steel, 20% H_2O, 5% boron is a near-optimal composition, from the standpoint of nuclear radiation attenuation, for a mixture of these three materials.) From results in Figs. 5 and 6 the following conclusions can be drawn:

1. Comparing the results for designs 101 and 112 and designs 102 and 116 shows that a 75% SS + 20% H_2O + 5% B is slightly better than a 50% SS + 50% B_4C shield mixture in terms of attenuation for a given thickness. Therefore, a helium-cooled shield will be thicker than a water-cooled shield by slightly more than the space required for helium coolant, i.e., ~5%.

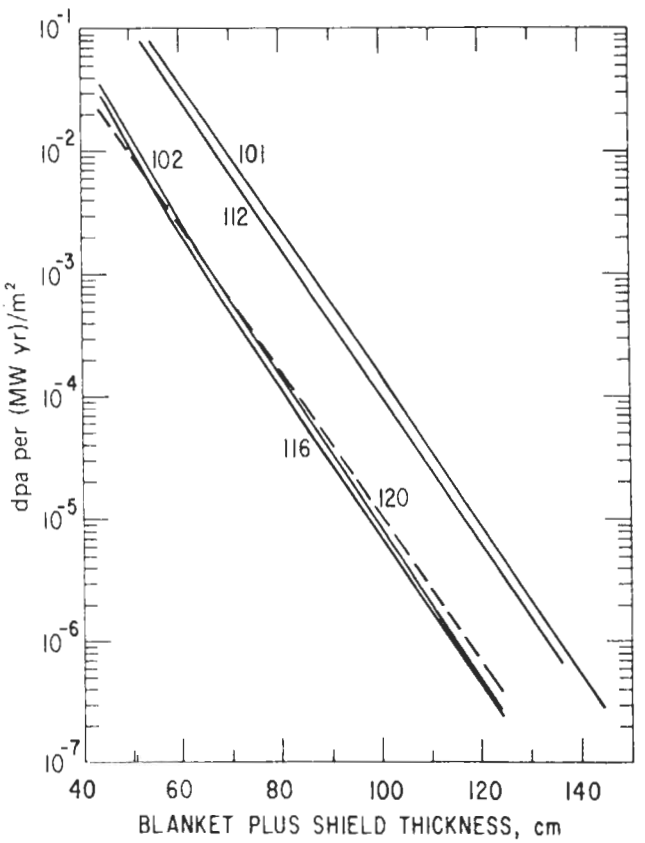

Fig. 5. Variation of atomic displacement in the magnet stabilizer (copper) with blanket plus shield thickness for designs in Set C.

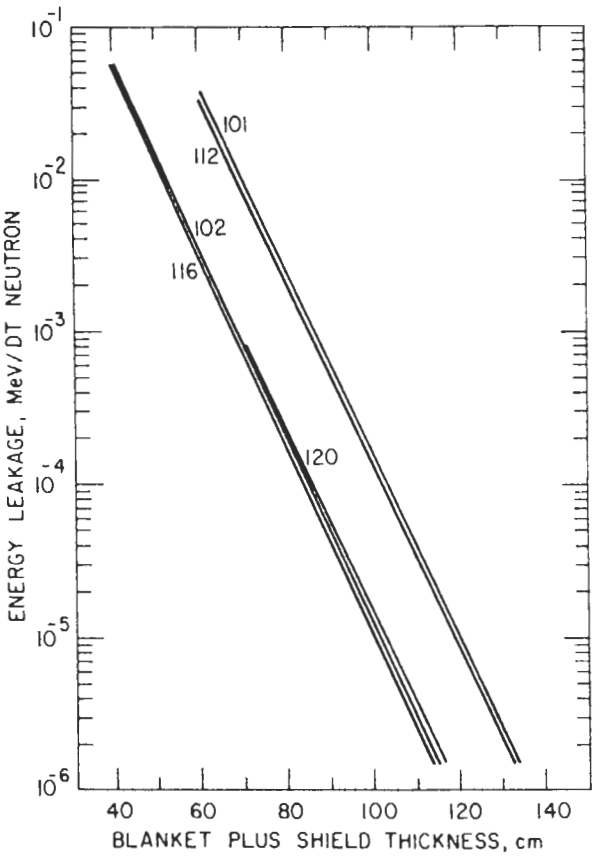

Fig. 6. Variation of total (neutron plus gamma-ray) energy leakage to the magnet with blanket plus shield thickness for designs in Set C.

2. Although a 75% + 20% H_2O + 5% B in the shield region is a slightly better attenuator than the 50% SS + 50% B_4C shield mixture, 100% stainless steel is a better attenuator than both mixtures in the blanket region. This can be seen from comparing results for designs 116 and 120 and from results to be given shortly for design set D. However, the space required for helium cooling in design 102 makes design 120 a preferable choice in terms of overall blanket plus shield thickness. To attenuate the radiation level such that the atomic displacement in the copper stabilizer is 1×10^{-4} dpa per (MW yr)/m^2 requires ~85 cm for both design 120 (water-cooled blanket and shield) and design 116 (helium-cooled blanket and water-cooled shield), and ~88 cm for design 102 (helium-cooled blanket and shield).

Therefore, using helium coolant in both the blanket and shield increases the blanket plus shield thickness by ~4% as compared to a water-cooled blanket and shield or a helium-cooled blanket coupled to a water-cooled shield.

Reactor size is particularly sensitive to the inner clearance between the plasma and the vertical segment of the D-shaped toroidal field coil. Space restrictions in other regions surrounding the plasma are much less severe. It appears very advantageous therefore, that the blanket/shield region in the space-limited zone be constructed of materials that are very efficient attenuators, e.g., tungsten-B_4C and tantalum-B_4C mixtures. Designs 102, 103, and 108 in design set D described in Table IV are used as the basis for comparing stainless steel with tungsten. The blanket/shield composition is 50% stainless steel + 50% B_4C in design 103, and 50% tungsten + 50% B_4C in design 108. The shield in design 102 is similar to that in design 103 but the blanket is 30-cm stainless steel. Figures 7 and 8 show the atomic displacement and energy leakage as a function of Δ_{BS} for the three designs. Using the tungsten-B_4C mixture saves ~12 to 15% on Δ_{BS} compared with the stainless-steel B_4C mixture. Results in Sec. IV also show that the tantalum-B_4C mixture is more effective than the stainless-steel B_4C mixture, but the tungsten-B_4C mixture is better than both.

Tungsten and tantalum have the combined problems of high cost, strong activation, and high density. The present material cost[22] of ~100$/kg

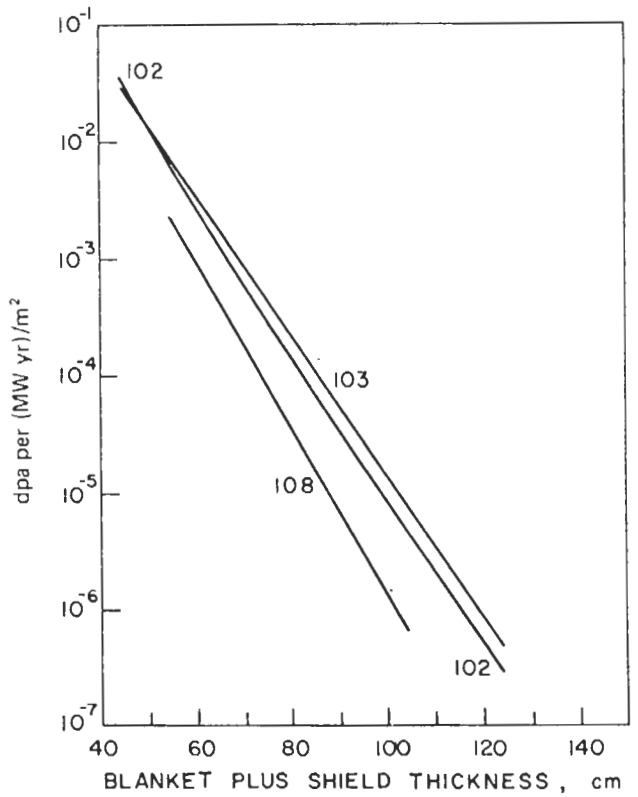

Fig. 7. Variation of atomic displacement in the magnet stabilizer (copper) with blanket plus shield thickness for designs in Set D.

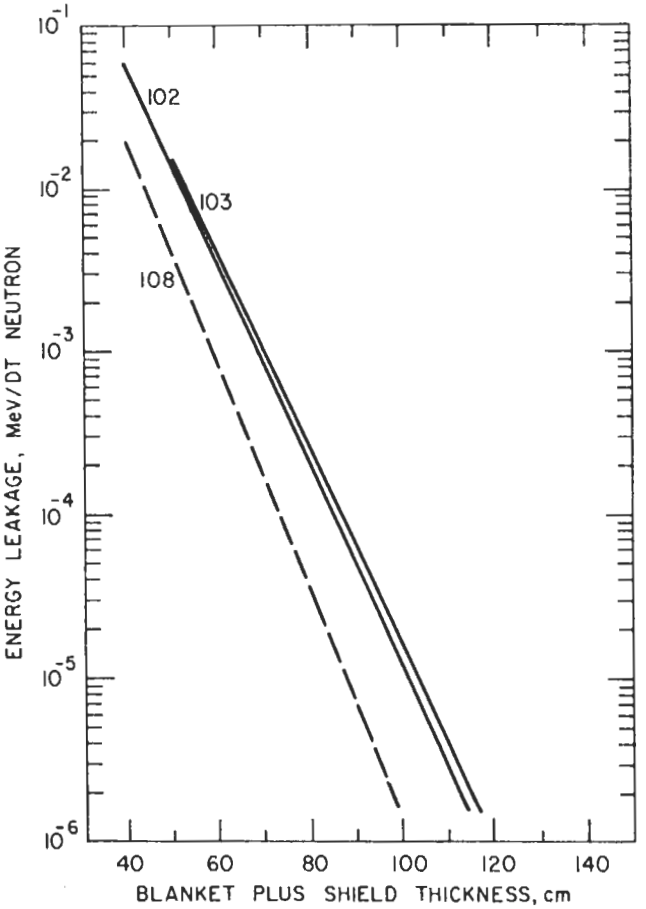

Fig. 8. Variation of total (neutron plus gamma-ray) energy leakage to the magnet with blanket plus shield thickness for designs in Set D.

for tungsten and tantalum is too expensive to justify its use in large quantities in the blanket/shield. However, their utilization in the inner blanket/shield in space-restricted and maximum magnetic field-limited machines such as a TEPR can be very advantageous in terms of reduced reactor size for a given power level. While tungsten and tantalum activate strongly, the presence of large amounts of boron carbide will eliminate most of the resonance and low-energy region neutron capture, and this will likely result in substantial reduction in tungsten and tantalum activation. Pure tungsten is very brittle and difficult to fabricate. However, there are several tungsten base alloys with 90 to 97% tungsten content, the balance being copper, nickel, or an iron-nickel mixture together with other additive elements.[23] Some of these alloys are reasonably ductile and can be fabricated.

Induced radioactivity in the blanket, magnet shield, magnet, containment vessel, and other reactor components is one of the important considerations in a Tokamak reactor design. Of particular concern in the TEPR design are the effects of induced activation on personnel access for routine maintenance and necessary repairs. The maximum concentration of radioactivity in the reactor occurs in the first wall. A crude estimate of the biological dose at shutdown in a location near a first wall operated to an integral wall loading of 0.5 (MW yr)/m^2 gives 1, 2, 3, and 6×10^8 mrem/h for aluminum, V–20 Ti, stainless steel, and Nb–5 Zr first wall materials, respectively. These values decrease, in the same order, to 100, 3×10^6, 1×10^8, and 5×10^7 mrem/h after a cooldown time of ~5 weeks. It is emphasized here that these estimates are very approximate and have one to two orders of magnitude uncertainty. However, comparing these values for the biological dose with a maximum permissible dose of 12 rem/yr for occupationally exposed individuals shows clearly that remote maintenance will be required for handling stainless-steel, niobium, and vanadium structures. Aluminum, and perhaps graphite, may require only a minimal degree of radiation protection. It should be noted that the radioactivity builds up very rapidly during operation and decays relatively slowly after shutdown in stainless steel, niobium, and vanadium. Thus the biological dose is not very sensitive (in an order of magnitude sense) to the operating time and duty cycle. In this context, extending the cooldown time from a few weeks to a few months will not help a great deal in easing remote maintenance.

There is an incentive to examine the possibility of constructing the blanket and magnet shield from low-activation materials such as aluminum or graphite to ease the remote maintenance requirements. The nuclear performance of these materials is examined by designs 102, 108, 113, 114, 117, 118, and 119 in design set E (see Table V). The atomic displacement in the magnet stabilizer and the energy leakage to the magnet in these designs are shown in Figs. 9 and 10 as functions of the blanket/shield thickness. The results in these figures can be summarized as follows:

1. Comparing the results for designs 113 and 117 and designs 114 and 118 shows that there is little difference between graphite and aluminum in terms of the required Δ_{BS} for a given attenuation.
2. Using 30 cm of aluminum (design 113) or graphite (design 117) in the blanket increases Δ_{BS}, for a given attenuation, by ~20% relative to a 30-cm stainless-steel blanket (design 102).
3. Both designs 114 and 118 with 30-cm blankets of aluminum and graphite, respectively, followed by 50% aluminum + 50% B_4C shields would require increasing Δ_{BS} by a factor of 2 to produce the same attenuation obtainable with a 30-cm stainless-steel blanket followed by 50% stainless steel + 50% B_4C shield (design 102).
4. Replacing the 30-cm stainless-steel blanket in design 102 by vanadium increases the required Δ_{BS} by ~8 cm.

A low induced activation system that consists of a 30-cm blanket of aluminum or graphite followed by a 50% aluminum + 50% B_4C shield would require Δ_{BS} to be ~140 cm to meet the magnet protection criteria discussed later. This is too thick to be acceptable in the inner high magnetic field region in a TEPR. The use of aluminum and graphite in the outer blanket/shield will depend on many other considerations in the design. There are other problems associated with the utilization of graphite and aluminum in the blanket. For example, graphite is subject to severe radiation damage when irradiated to high fluences. An aluminum blanket imposes on the design a low operating temperature (300 to 400°C) and a tenuous safety factor for blanket meltdown (aluminum melts at ~660°C).

III. IMPORTANT CONSIDERATIONS IN OPTIMIZING THE BLANKET/SHIELD DIMENSIONS

As indicated earlier, the size and cost of a Tokamak reactor is sensitive to the dimension of the total clearance between the plasma and the toroidal field coils. To keep the size of the TEPR

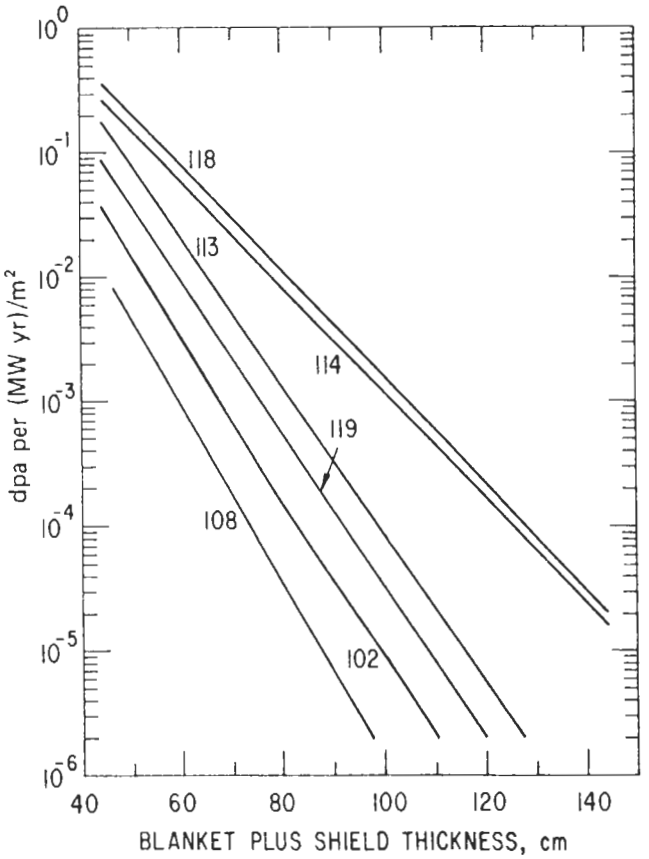

Fig. 9. Variation of atomic displacement in the magnet stabilizer (copper) with blanket plus shield thickness for designs in Set E.

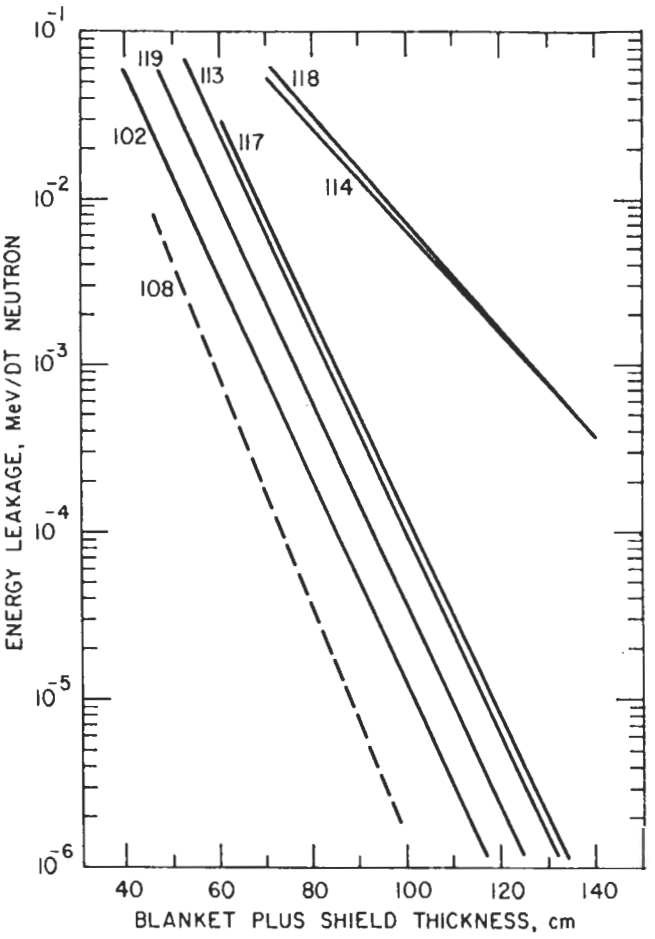

Fig. 10. Variation of total (neutron plus gamma-ray) energy leakage to the magnet with blanket plus shield thickness for designs in Set E.

at a reasonable level (major radius ~5 to 7 m) and in the meantime produce a significant amount of power output, particular attention has to be given to optimizing the blanket/shield thickness. The magnitude of nuclear attenuation required by the magnet protection criteria cannot be compromised beyond the tolerable level for satisfactory operation of the superconducting magnet. As is discussed in this section, experiments have shown that a substantial part of the radiation damage to the magnet can be recovered by annealing at elevated temperatures. However, magnet cooldown from room temperature to 4.2 K takes a long time (~2 to 3 months). Therefore, magnet protection criteria are, in some sense, related to many aspects of the overall design criteria for the reactor, e.g., the duty cycle. Besides the magnet protection, the electrical power required to run the refrigerators represents another constraint that also favors increasing the blanket and shield thickness. In the following subsections, these trade-off considerations are examined in some detail.

III.A. Magnet Protection Criteria

Since radiation damage to the magnet plays an important role in determining the size of the blanket shield system, quantitative correlations between the magnet damage and nuclear radiation levels need to be established. The magnet components of concern here are (a) the superconductor, (b) the normal (stabilizing) conductor, (c) thermal and electrical insulators, and (d) structural materials.

Limited, but very useful, information about the neutron irradiation effects on the magnet conductors have accumulated from experimental studies (see for example Refs. 24 through 28) in the last few years. Many of these experiments were made at liquid-helium temperatures; therefore, the results are applicable for superconducting magnets. The neutron spectrum, however, resembles in most cases a fission spectrum or

softer. Such a spectrum is adequate for simulating neutron spectra in the superconducting magnets for large reactors where the blanket and shield may be 1.5 to 2 m with attenuation factors[12] of $\sim 10^6$ to 10^8. The neutron spectrum in a TEPR magnet with a blanket/shield of ~0.7 to 1 m, however, has a large component of high-energy neutrons. Many experiments have been performed at ANL's low-temperature, fast-flux facility.[27] Figure 11 shows three neutron spectra A, B, and C. Curves A and B represent the neutron spectrum in the magnet for 60- and 100-cm blanket/shield of stainless steel and boron carbide arranged in zones similar to that of the reference design described in Sec. IV. Curve C represents the neutron spectrum for the ANL low-temperature fast-flux facility. Figure 12 shows

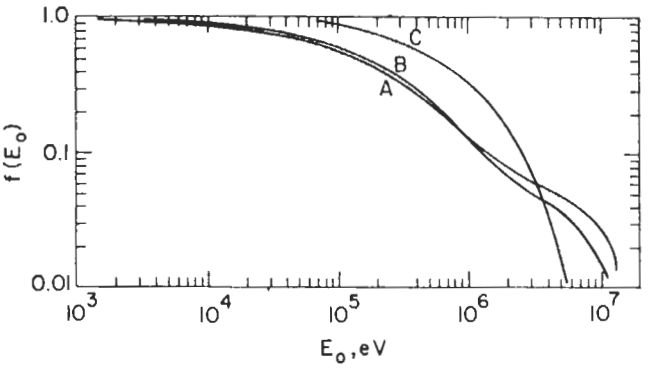

Fig. 12. The fraction, $f(E_0)$, of the total neutron flux with neutron energies above E_0, as a function of E_0. Curves A and B are for the flux outside a stainless-steel B_4C blanket/shield of 60- and 100-cm thickness, respectively. Curve C is for the flux in ANL Low-Temperature Facility.

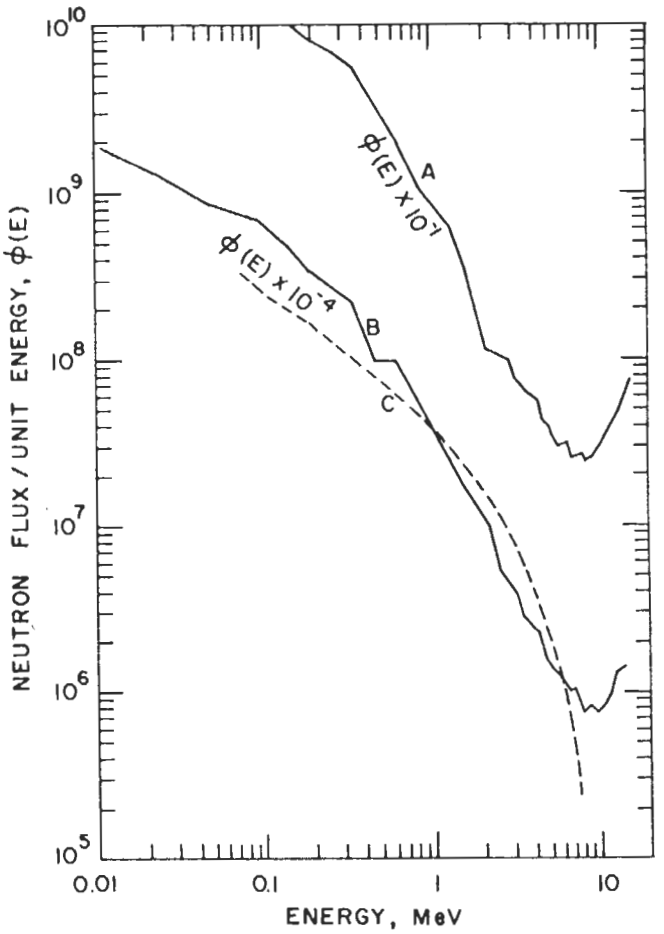

Fig. 11. Comparison of neutron spectrum in TEPR toroidal field magnet and neutron spectrum used in radiation damage measurements. A - Neutron spectrum in the magnet for 60-cm SS-B_4C blanket/shield. B - Neutron spectrum in the magnet for 100-cm SS-B_4C blanket/shield. C - Neutron spectrum for the ANL Low-Temperature Facility (Ref. 27). (A and B normalized to $W_n = 0.2$ MW/m^2.)

the fraction, $f(E_0)$, of the total neutron flux with neutron energies above E_0, as a function of E_0 for the same three fluxes, A, B, and C. From the two figures, it can be seen that a typical fission spectrum such as that of C can simulate very well the neutron spectrum in a TEPR magnet for neutrons of energies below ~5 MeV. The fraction of neutrons above 0.1 MeV in C (90%) is greater than in A and B (~60%). However, the fission spectrum (C) has a very small component (1.5%) above 5 MeV and essentially no neutrons above 8 MeV. The TEPR magnet spectra (A and B) have ~5% of the neutrons of energies >5 MeV. Many neutron-induced reactions [e.g., (n,α), (n,p), $(n,n'p)$, etc.] occur only at high energies. Furthermore, for a given reaction, the recoil energy generally increases with the neutron energy. Therefore, high-energy neutrons are more capable of producing lattice damage than low-energy neutrons. Consequently, extrapolation of present experimental results on liquid-helium temperature irradiation to superconducting magnets in a fusion reactor with relatively thin blanket/shield should be exercised with care. A design safety factor on the neutron dose-related radiation damage parameters in the magnet seems necessary at present.

III.B. Irradiation Effects in Superconductors

Experimental studies on the effects of low-temperature neutron irradiation on the properties of superconducting materials have been reported in Refs. 24 through 28. Both NbTi and Nb_3Sn have been proposed for fusion reactor superconducting magnets. The NbTi superconductor is currently the preferred choice for TEPR because of its ductility and the unparalleled experience in its fabrication and use in superconducting magnets.

Although Nb_3Sn is capable of producing much higher magnetic fields than NbTi, further developments for its utilization in large superconducting magnets are required.

The most important property in the behavior of a superconducting material under irradiation is its critical current density, J_c. The influence of radiation damage on J_c in commercial NbTi and Nb_3Sn was found to depend greatly on many factors such as the metallurgical structural (hence, initial J_c) of the samples irradiated. The critical current density of NbTi shows mostly a decrease. Depending on the position of the maximum pinning force[28] (product of the critical current density and the magnetic induction), a decrease in J_c of ~1 to 10% was observed for irradiation up to 3×10^{18} n/cm^2. Many of the Nb_3Sn samples[28] irradiated at low temperatures showed an increase in the critical current density at low neutron fluences. The increase has a maximum at a dose of $\sim 5 \times 10^{17}$ n/cm^2, and at higher doses J_c decreases. Annealing experiments showed that a considerable recovery of the radiation damage in NbTi and Nb_3Sn can be reached at room temperature.

Decreasing the allowable current density, J_c, involves an increase in the magnet capital cost to produce a specified magnetic field. By proper selection of the initial conditions for the NbTi and Nb_3Sn, the maximum decrease in J_c can be limited to <5% for irradiation up to 3×10^{18} n/cm^2. A few percent decrease in J_c represents only a small increase in the magnet cost and can also be accommodated by decreasing the liquid-helium temperature a fraction of one degree Kelvin.

The total neutron flux at the magnet, ϕ_m, is related to the total neutron flux at the first wall, ϕ_w, by the relation

$$\phi_m \approx \phi_w \exp(-\mu x) \quad , \tag{3}$$

where x is the blanket plus shield thickness and μ is the total flux attenuation coefficient. If the maximum total fluence at the magnet is restricted to $\sim 3 \times 10^{18}$ n/cm^2, then

$$\exp(-\mu x) < \frac{1.4 \times 10^{-4}}{W_n \cdot t} \quad , \tag{4}$$

where W_n is the neutron wall loading in MW/m^2 and t (in years) is the irradiation period or the time span between magnet anneals multiplied by the duty cycle. The product of W_n and t is called the integral wall loading, I_w, and is used frequently here in units of (MW yr)/m^2. Figure 13 shows the total neutron flux at the magnet as a function of blanket plus shield thickness for 50% stainless steel + 50% B_4C composition and a neutron wall loading of 0.2 MW/m^2. From this figure and Eq. (4), it can be seen that a blanket/shield of 50% stainless steel + 50% B_4C should be >65 cm for irradiation up to an integral wall loading of 1 (MW yr)/m^2.

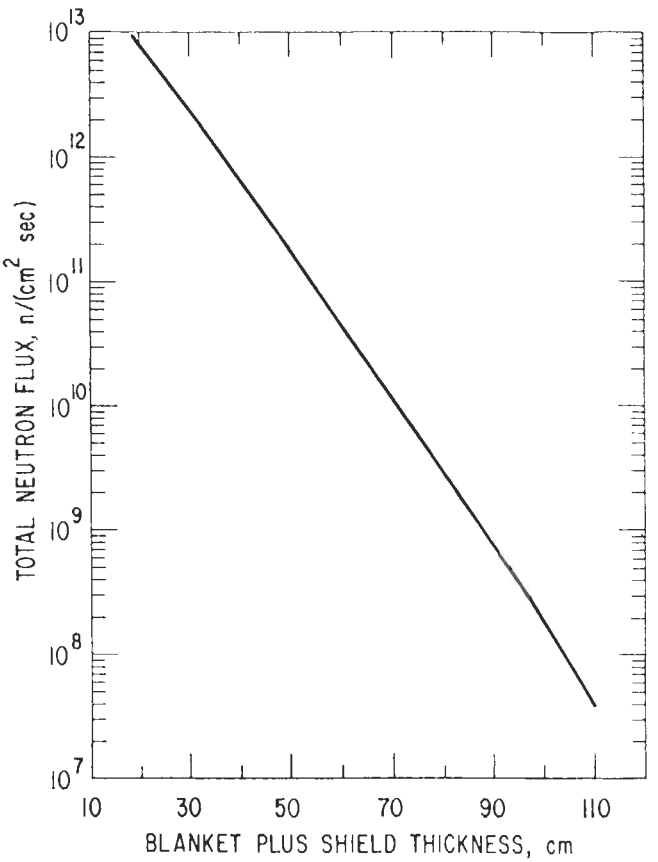

Fig. 13. Total neutron flux as a function of blanket plus shield thickness for 50% SS + 50% B_4C composition and a neutron wall loading of 0.2 MW/m^2.

III.C. Irradiation Effects on Stabilizing Material

Stabilizing superconducting magnets requires forming the superconductor into a composite with a sufficient amount of high-conductivity normal metal usually called stabilizing material. Copper and aluminum are the most likely candidates for stabilizing materials. Cryogenic stabilization criterion requires[29] that the heat transfer from the stabilized superconducting matrix must be sufficient to transfer the I^2R heat generated in the stabilizing material when a flux jump occurs, i.e.,

$$I^2\rho < aPq \quad , \tag{5}$$

where

I = operating current

ρ = resistivity of the stabilizing material

a - normal conductor cross-sectional area

P = cooled perimeter of the composite

q = maximum allowable heat flux in W/cm^2.

This shows that an increase in the resistivity of the stabilizing material results in a decrease in the allowable operating current to keep the cryogenic stability criterion satisfied.

Neutron irradiation of high-purity metals near liquid helium temperatures showed a significant increase in the electrical resistivity. The rate of increase in the radiation-induced resistivity, $d\rho_r/dt$, was found to vary almost linearly with the radiation-induced resistivity, ρ_r, i.e.,

$$\frac{d\rho_r}{dt} = \alpha(\rho_s - \rho_i) \quad , \tag{6}$$

$$\rho_r = \rho_s[1 - \exp(-\alpha t)] \quad , \tag{7}$$

where t is the irradiation time and ρ_s and α are experimentally determined parameters for each metal. Although some nonlinear defect production rates have been observed, the scatter in the experimental data does not justify[30] a better fit than that in Eq. (6). The value of ρ_s can be determined to within 10 to 50% accuracy[27] and is $\sim 3 \times 10^{-7}$ and 8×10^{-7} Ω-cm for copper and aluminum, respectively.

The parameter α in Eq. (7) is a characteristic of the metal and depends on the magnitude and energy dependence of the neutron spectrum. To relate the radiation-induced resistivity in the stabilizing material to other parameters of the reactor, the product of αt should be expressed in a form that is fairly independent of the neutron spectrum. Since the increase in the resistivity is due to production of defects, the choice of number of displacements per atom (dpa) as a measure of irradiation dose is justified. The latest experimental data of Brown et al.[27] were used to derive the following formula for radiation-induced resistivity in copper:

$$\rho_r = 3 \times 10^{-7}[1 - \exp(-563d)] \ \Omega\text{-cm} \quad , \tag{8}$$

where the saturation resistivity for copper, ρ_s, is equal to 3×10^{-7} Ω-cm and d is the total number of atomic displacements. This formula agrees with other experimental data to ±10% for $10^{-8} < \rho_r < 10^{-7}$. Outside this range, a maximum deviation of 50% was observed. The displacement cross sections for copper used in deriving the above formula are those used in the previous section. Current methods for calculating displacement cross sections have limited accuracy. However, in calculating ρ_r in any given system, the results will be most accurate if the same displacement cross sections employed in deriving the above formula are used. The value of the displacement energy has no effect except through normalization of the numerical factor (563) in the exponent of the exponential term of Eq. (8). The accuracy of the above expression, however, will be affected strongly by the accuracy of the energy dependence of the displacement cross sections when the neutron spectrum is markedly different from that used in the experimental measurements.

Experimental studies have shown that full recovery of the radiation-induced resistivity can be accomplished by heating aluminum to ~260 K and copper to ~400 K. Partial recovery occurs at lower temperatures. The amount of recovery at various temperatures depends to some extent on the irradiation neutron spectrum. For fast-neutron irradiation, 31, 61, and 95% recovery of the radiation-induced resistivity in copper occurs when it is heated up to 50, 170, and 320 K, respectively.[26] For aluminum, 40 and 60% recovery are obtainable at 52 and 200 K, respectively. Since the specific heat for these metals increases with temperature, substantial savings in the power requirements to cool down the magnet can be made by warming the magnet up only to temperatures just enough for ~70 to 80% recovery.

The consequences of a superconducting magnet for a fusion reactor going normal have not yet been fully assessed. However, they are very likely to be grave because of the tremendous amount of stored energy and the relatively high levels of radioactivity in the reactor components. Thus, it is generally accepted that the superconducting coils for the TEPR must be cryogenically stable. In addition to ensuring the stability of the superconductor composite, provisions must be made to prevent damage to the coils under any condition of malfunction. For example, by connecting the coils in series with a dump resistor between every two neighboring coils, the energy can be removed fast enough and without accumulating a large voltage with respect to the ground.[31] The increase in the resistivity of the stabilizing material can be accommodated without violating the cryogenic stability constraint of Eq. (5) by lowering the operating current, increasing the heat flux, q, and/or modifying the conductor design. Reduction of the operating current is undesirable, and the heat flux is limited by the rate of heat transfer to liquid helium. Therefore, modifying the conductor design is usually the preferred choice. If we assume the conductor thickness is t and the conductor width is W, then $a = tW$, and for one-face cooling (or 50% both-face cooling) $P = W$. Thus, the resistivity increase can best be accommodated by increasing W. However, fabrication difficulties place a limit on the conductor aspect ratio (W/t). It should be noted that due to neutron attenuation inside the magnet, the dpa, and hence ρ_r, will vary with

position within the magnet. Changing the dimensions from one conductor to another radially in the magnet will increase the fabrication cost. On the other hand, since the modulus of elasticity for copper at 4.2 K is about half that of stainless steel, the amount of structure (typically stainless steel) can be reduced by about half the increase in copper.

Design of superconducting magnets involves many complicated trade-off and optimization considerations in addition to several stringent constraints.[32,33] Therefore, it is difficult at present to set an upper feasible limit on the increase in the resistivity of stabilizing materials. Future studies are needed in this regard and also to correlate the increase in cost to changes in the amount of conductor for typical TEPR design parameters.

The maximum allowable increase in the resistivity of the stabilizer due to neutron irradiation affects the blanket plus shield thickness, Δ_{BS}, for a given power level and blanket/shield composition. The intrinsic plus magnetoresistivity of copper at 80 kG is $\sim 4.6 \times 10^{-8}$ Ω-cm. A radiation-induced resistivity of 3×10^{-8} Ω-cm represents a 65% increase in the resistivity of copper at 80 kG and would require a change of the conductor cooling surface width by <30% to keep the operating current the same. Such modification can practically be made without much difficulty. A ρ_r of 3×10^{-8} is 10% of the saturation resistivity for copper and is reached at 1.87×10^{-4} dpa. Table VI shows the minimum blanket plus shield thickness required to protect the magnet such that the maximum dpa at the inner winding does not exceed 1.87×10^{-4} for various integral wall loading. The calculations are based on blanket/shield composition of 50% stainless steel + 50% B_4C. The integral wall loading is the product of the neutron wall loading, operating time, and duty cycle. Most of the values for the operating time in the table represent practical choices for time span between magnet anneals for full recovery. The duty cycle includes the plasma cycle and plant availability factors and is varied from 20 and 50 to 80%. It is very unlikely that a duty cycle >50% can be accomplished with an experimental power reactor. The neutron wall loading is varied from 0.1, 0.2, and 0.5 to 1 MW/m^2. It was assumed in deriving the results in Table VI that variation of power

TABLE VI

Dependence of Blanket Plus Shield Thickness and Refrigerator-Power Requirements on Integral Wall Loading if the Maximum Allowable Radiation-Induced Resistivity in the Stabilizing Copper Conductor is 3×10^{-8} Ω-cm

Case	Neutron Wall Loading (MW/m^2)	Span Between Magnet Anneals (yr)	Duty Cycle (%)	Integral Wall Loading [(MW yr)/m^2]	Blanket Plus Shield Thickness[a] (cm)	Refrigerator Power[b] (%)
1	0.1	2	20	0.04	59	113
2	0.1	2	50	0.10	67	33
3	0.1	2	80	0.16	71.5	18
4	0.1	5	80	0.40	77	9
5	0.1	20	80	1.60	87.5	1.5
6	0.2	2	20	0.08	65	3.3
7	0.2	2	50	0.20	72.5	16
8	0.2	2	80	0.32	75.5	11
9	0.2	5	80	0.8	81	6
10	0.2	20	80	3.2	92.5	1
11	0.5	2	20	0.20	72.5	16
12	0.5	2	50	0.50	78.5	7.5
13	0.5	2	80	0.80	81.0	6
14	0.5	5	80	2.0	89	1.4
15	0.5	20	80	8.0	97	0.6
16	1.0	5	80	4.0	93.5	1
17	1.0	20	80	16.0	107	0.15

[a] Based on optimized blanket and shield composition of stainless steel and boron carbide; the calculations allowed a void fraction (for helium cooling, thermal expansion, etc.) of 10 vol% in the first 40 cm, and 5% in the rest of the shield.

[b] Refrigeration electric-power requirements expressed in percentage of plant electric-power output. Assumptions: 70% of the outer surface area covered by the magnet, plant thermal efficiency of 30%, 16.5 MeV are recoverable for each fusion reaction, and 500-W electrical power required per watt of thermal-power input to the refrigerators.

with time has no effect on the radiation-induced resistivity except through the accumulated dpa and, hence, the integral wall loading.

Table VI shows that if the maximum allowable ρ_r in copper is 3×10^{-8} Ω-cm, the blanket plus shield thickness for 50% stainless steel + 50% B_4C mixture varies from 59 to 107 cm as the integral wall loading is varied from 0.04 to 16 (MW yr)/m^2. For a given blanket/shield composition and dimensions, the fraction of electrical power required to run the refrigerators of the superconducting magnet can be calculated using the results of the previous section and a few reasonable assumptions. Table VI shows this fraction for each Δ_{BS}. The assumptions made in deriving this quantity were: (a) 70% of the outer surface area covered by the magnet; (b) plant thermal efficiency is 30%; (c) recoverable energy per fusion reaction is 16.5 MeV; and (d) 500 W of electric power are required per watt of thermal input to the refrigerators. These are typical values that can vary by as much as 50% and, of course, the refrigeration power requirements will vary accordingly. From the results in the table, it can be seen that the fraction of electrical power required to run the refrigerators, f_r, varies from over 100% to <1% when Δ_{BS} is varied from 60 to 100 cm. Economics considerations[12] limit f_r in commercial power reactors to <0.1%. However, the cost per unit power output in a TEPR device is not as important as the total capital cost. Cryogenic refrigerators currently cost ~0.5 million dollars/kW of the refrigeration capacity. Thus, for 150 MW(th) an f_r of 0.1 corresponds to a capital cost of the refrigerators of ~4 million dollars and operating cost of ~0.5 million dollars per year of continuous operation. Therefore, an f_r as high as 10% can be tolerated. Increasing f_r beyond 10% is costly, creates problems of power supply for the refrigerators, and affects the reliability of the magnet.

The results of Table VI show that decreasing the integral wall loading reduces Δ_{BS} required to limit ρ_r in the copper stabilizer to 3×10^{-8} Ω-cm. However, decreasing Δ_{BS} increases the refrigerators' power requirement significantly and in a few cases to intolerable levels. Therefore, for low integral wall loading, the refrigerator power requirements can be more limiting on the blanket/shield design than the increase in the resistivity of the stabilizer. For a given neutron wall loading, decreasing the duty cycle and the time span between magnet anneals reduces the cumulative damage in the magnet but does not affect the refrigerator power requirements.

The results in Table VI are based on a uniform blanket/shield surrounding the plasma. The refrigeration power requirements, however, can be reduced substantially by increasing the blanket/shield thickness in the outer regions where space restrictions are much less severe than in the inner high-magnetic-field region as discussed in detail in the next section.

IV. BLANKET/SHIELD FOR THE ANL-TEPR REFERENCE DESIGN

The foregoing considerations were the basis for the nuclear design of a blanket/shield system for the ANL preliminary conceptual design for a Tokamak Experimental Power Reactor, called ANL-TEPR. The reactor is designed for staged operation as described in Sec. II and its thermal power is 130 MW. The nuclear design of the blanket/shield for Stage I of the ANL-TEPR is described in this section and the neutronics-related results are analyzed in detail. The primary design criteria were:

1. radiation-induced resistivity increase in the copper stabilizer of the superconducting toroidal field coils $<3 \times 10^{-8}$ Ω-cm
2. maximum decrease (due to irradiation) in the critical-current density in NbTi superconductor in the toroidal-field coils <5%
3. maximum power required to run the refrigerators of the superconducting toroidal field coils ~1% of plant electrical-power output
4. total radiation dose to the Mylar insulation of the toroidal-field coils $<1.2 \times 10^8$ rad for the magnet lifetime
5. a safety factor to be applied in the design particularly for the magnet radiation damage-related neutronics parameters. This safety factor is a variable that is derived for each quantity from estimates of uncertainties.

This reference design does not represent a fully detailed final design of the blanket and shield for a TEPR. However, the analysis of such a design serves three important purposes:

1. It demonstrates the feasibility of designing a TEPR blanket/shield system that satisfies the major requirements of such a system.
2. A knowledge of the major characteristics and key parameters of such a conceptual design is very helpful in understanding the major problems of the primary energy conversion system and its interface with other reactor components.
3. This design provides a reasonable starting point for additional in-depth optimization and detailed design studies.

Figure 14 is a schematic of the ANL-TEPR reference design for the blanket and shield. No modular or cellular structure is shown in this figure. However, the figure illustrates a new concept that is proposed for the TEPR design. The inner region between the plasma and the vertical segment of the D-shaped toroidal-field coils comprises the highest magnetic field zone inside this coil system. As discussed earlier, for a given maximum magnetic field at the magnet, reducing the blanket/shield thickness in this inner high-magnetic-field region increases the reactor power significantly and also makes it possible to reduce the size of the reactor for the same reactor power. In the exterior region of the D-magnet, the space problems are greatly reduced by the fact that extending the D in the low-magnetic-field region, hence low-stress region, does not involve a large cost penalty or an added technological difficulty. Therefore, a blanket/shield system is proposed that consists of two parts. The first part is a specially designed blanket/shield region in the inner clearance between the plasma and the vertical segment of the D-shaped magnet, and the

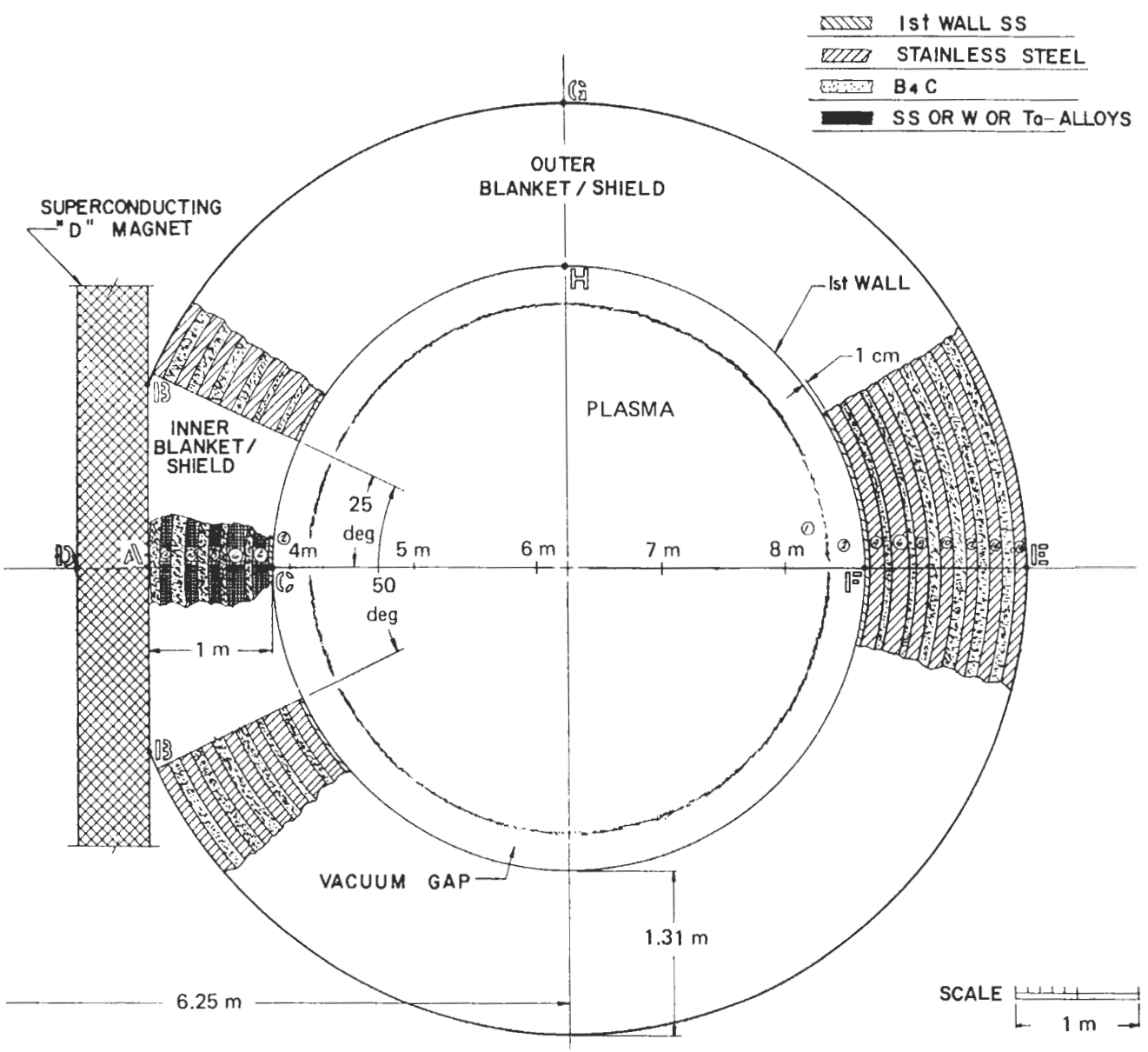

Fig. 14. Vertical section of the blanket/shield for the ANL-TEPR reference design. (Toroidal-field coil bore is 7.7 m; the additional space of 59 cm between the outer blanket/shield and the D-shaped magnet is provided for access, assembly, disassembly, etc.)

second part is the blanket/shield in the outer regions. The inner part is designed to minimize the blanket/shield thickness in the high-magnetic-field region to a value that just satisfies the radiation-damage design requirements in the magnet. This is accomplished by using materials that are very efficient attenuators, such as tungsten or tantalum. Although these materials are very expensive, the increase in the blanket/shield cost is not large because the total volume of the inner region in this concept is only 5 to 10% of the total blanket/shield volume. The small increase in the blanket/shield cost is more than offset by the reduction in the total reactor cost, as is discussed later.

The inner region of the blanket/shield is generally not useful as a test module in any practical design because of the lack of space between the magnets at the inner side of the torus. Therefore, the criterion of reducing blanket/shield activation and biological dose after shutdown can be significantly relaxed and a wider spectrum of materials can be considered for this region. The outer blanket/shield is the major component of the blanket/shield system. Space restriction in the outer region is not severe in a D-shaped magnet, and the use of materials less efficient and less expensive than those used in the inner blanket/shield is possible.

TABLE VII

Dimensions and Material Composition of the ANL-TEPR Inner Blanket/Shield

Zone	Outer Radius (cm)	Thickness (cm)	Material Composition	Density Factor[a]
1	210	210	Plasma	0.0
2	240	30	Vacuum	0.0
3	241	1	Stainless steel	0.5
4	256	15	Stainless steel	0.9
5	261	5	Boron carbide[b]	0.9
6	276	15	Stainless steel	0.9
7	281	5	Boron carbide	0.9
8	291	10	Stainless steel	0.95
9	301	10	Boron carbide	0.95
10	311	10	Stainless steel	0.95
11	321	10	Boron carbide	0.95
12	331	10	Stainless steel	0.95
13	340	9	Boron carbide	0.95
14[b]	397	57	Magnet[c]	1.0

[a] This density factor was used in the neutronics calculations to account for space occupied by the helium coolant, thermal expansion, material packing density, etc.

[b] Boron carbide (B_4C) with boron of natural isotopic composition.

[c] The superconducting magnet was homogenized in the neutronics calculation as 44% copper, 44% stainless steel, 6% NbTi, and 6% helium (these are volume percentages).

IV.A. Neutronics and Photonics Analysis of the Blanket and Magnet Shield

Figure 14 shows both the inner and outer blanket and magnet shield for the reference design. The major radius is 6.25 m and the first wall radius is 2.4 m. The thickness of the inner blanket/shield (distance between points A and C in the figure) is 100 cm. The thickness of the outer blanket/shield (distance between points F and E in the figure) is 131 cm. Dimensions and material compositions for the inner and outer blanket/shield are shown in Tables VII and VIII, respectively. The blanket and shield consist mainly of alternating zones of stainless steel and boron carbide. The dimensions and compositions of the various zones are the result of an attempt to maximize the attenuation for an inner blanket/shield thickness of 1 m of stainless steel and boron carbide. From results in Sec. II, a mixture of stainless steel and boron carbide was found superior (from the total attenuation standpoint) to all other material compositions investigated in

TABLE VIII

Dimensions and Material Composition of the ANL-TEPR Outer Blanket/Shield

Zone	Outer Radius (cm)	Thickness (cm)	Material Composition	Density Factor[a]
1	210	210	Plasma	0.0
2	240	30	Vacuum	0.0
3	241	1	Stainless steel	0.5
4	256	15	Stainless steel	0.9
5	261	5	Boron carbide[b]	0.9
6	276	15	Stainless steel	0.9
7	281	5	Boron carbide	0.9
8	291	10	Stainless steel	0.95
9	301	10	Boron carbide	0.95
10	311	10	Stainless steel	0.95
11	321	10	Boron carbide	0.95
12	331	10	Stainless steel	0.95
13	340	9	Boron carbide	0.95
14	351	11	Stainless steel	0.95
15	361	10	Boron carbide	0.95
16	371	10	Stainless steel	0.95
17[c]	430	59	Vacuum[c]	0.0
18[d]	487	57	Magnet[d]	1.0

[a] This density factor was used in the neutronics calculations to account for space occupied by the helium coolant, thermal expansion, material packing density, etc.

[b] Boron carbide (B_4C) with boron of natural isotopic composition.

[c] This space allows for assembly and replacement of the various modules. Parts of this region will be occupied by accessory equipment.

[d] The superconducting magnet was homogenized in the neutronics calculation as 44% copper, 44% stainless steel, 6% NbTi, and 6% helium (these are percentages on volume basis).

this study except tungsten-boron carbide and tantalum-boron carbide mixtures. Furthermore, stainless steel is a good structural material, and there exists a great deal of experience with its fabrication. These considerations make stainless steel a good choice for the first wall and structure as well as the basic neutron and gamma-ray attenuator in the blanket/shield in TEPR. The nucleonic results for the reference design are discussed next. The effects of reducing the inner blanket/shield thickness to less than the reference value of 1 m is examined in Sec. IV.D. Alternative designs that bring up the advantages of replacing the SS-B_4C in the inner blanket/shield by W-B_4C and Ta-B_4C mixtures are also investigated.

The maximum radiation damage and heat-generation rates in the magnet will occur at the intersection of the inner vertical segment of the D-shaped coil with the horizontal midplane (projected as point A in Fig. 14). Thus, the magnet design should be based on the values for the important parameters (e.g., radiation-induced resistivity, nuclear heating, and dose to the insulators) along the line A-D in Fig. 14. Therefore, in presenting the results for the reference design, great emphasis will be given to the inner region (i.e., line C-A-D). It should be noted that the first 100 cm of the outer blanket/shield is identical in the reference design to the inner blanket and shield. The difference in the neutronics results for the first meter of the outer blanket/shield (e.g., along line F-E or H-G) from those for the inner blanket/shield (line C-A) is very small. The level of nuclear radiation in the outer segment of the magnet is approximately two orders of magnitude lower than that in the inner segment.

The neutron, gamma, and total nuclear heating are given by zone in Table IX. The spatial distribution of these heating rates in the blanket and magnet shield are given in Figs. 15 and 16, respectively, for a neutron wall loading, W_n, of 0.2 MW/m^2. It is noted from these results that ~99% of the nuclear heating is generated in the first 40 cm; therefore, these 40 cm define the blanket according to the criteria given in the introductory section. Table IX shows that the total nuclear heating per DT neutron is 13 MeV. Hence, the total energy per fusion reaction (including the 3.5-MeV alpha) is ~16.5 MeV, which is substantially less than a typical value of 20 MeV found[21,34] for systems utilizing lithium. Using nuclear data from ENDF/B-IV increases the energy per fusion by ~1.5 MeV. Thus, there is uncertainty in the value of the total energy per fusion reaction reported here of ~10%. (This will be examined in greater detail in future studies.) In any event, the reduction in the energy per fusion when lithium is replaced by stainless-steel boron carbide mixture in a fusion reactor blanket is not surprising. Almost all the high-energy reactions in iron, chromium, and nickel are endothermic causing a relatively large-energy loss (converted to mass). Although each radiative capture in iron, chromium, and nickel results in an energy gain of ~8 MeV compared with 4.8 MeV in ^{6}Li(n, t) reaction, only ~20% of the neutrons in the

TABLE IX

Total Heating by Zone for the Inner Blanket/Shield of the ANL-TEPR Reference Design

Zone	Composition	Thickness (cm)	Density Factor	Neutron Heating	Gamma-Ray Heating	Total Heating	Total Heating (W/cm)[a]
				(in units of MeV/D-T neutron)			W_n = 0.2 MW/m^2
1	Plasma	210	0	---	---	---	---
2	Vacuum	30	0	---	---	---	---
3	SS	1	0.5	0.3057	0.4309	0.7366	1.5766(+3)
4	SS	15	0.9	2.5861	5.8210	8.4071	1.7995(+4)
5	B_4C[b]	5	0.9	2.3906	0.1274	2.5180	5.3895(+3)
6	SS	15	0.9	0.1662	0.6219	0.7881	1.687 (+3)
7	B_4C	5	0.9	0.3367	0.0126	0.3493	7.476 (+2)
8	SS	10	0.95	0.0108	0.0489	0.0597	1.2778(+2)
9	B_4C	10	0.95	0.0576	0.0029	0.0605	1.2949(+2)
10	SS	10	0.95	0.00065	0.00381	0.00446	9.546
11	B_4C	10	0.95	0.0026	0.00002	0.00262	5.607
12	SS	10	0.95	4.60 (−5)[c]	2.714(−4)	3.174(−4)	0.6794
13	B_4C	9	0.95	1.30 (−4)	1.354(−5)	1.435(−4)	0.3071
Sum				5.855	7.070	12.925	2.766 (+4)

[a] Total heating by zone in units of W/cm in the toroidal direction for a neutron wall loading of 0.2 MW/m^2.
[b] B_4C - boron carbide.
[c] 4.60(−5) = 4.60 × 10^{-5}, etc.

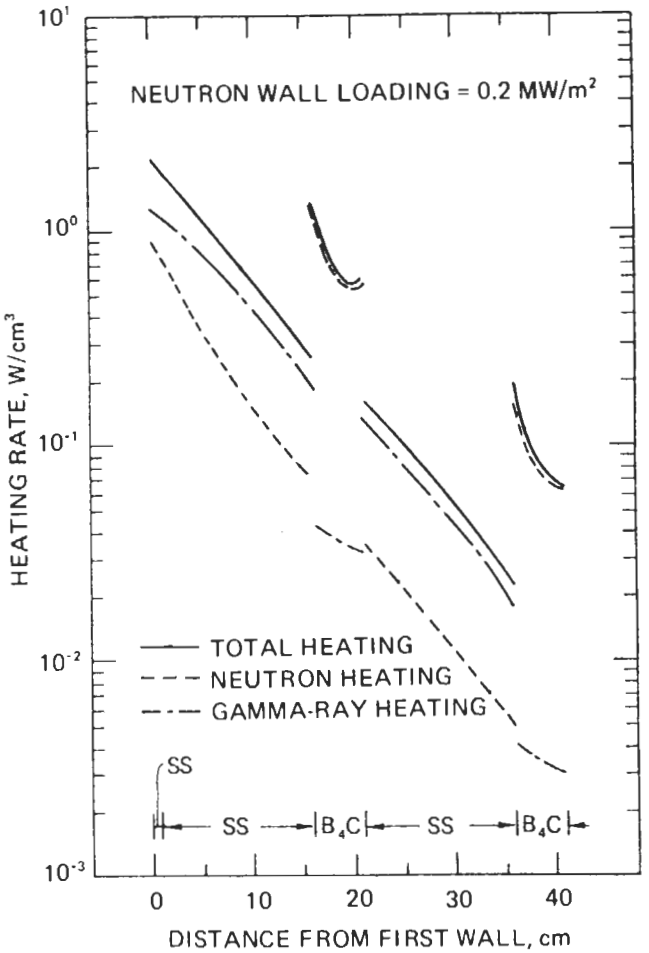

Fig. 15. Spatial distribution of heating rates in the ANL-TEPR blanket.

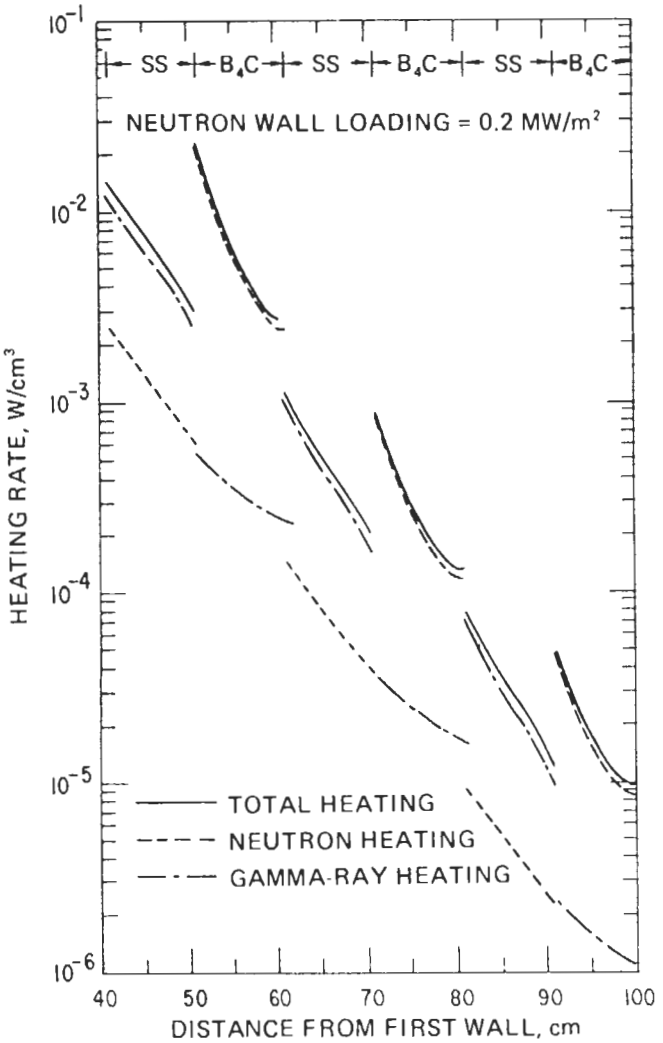

Fig. 16. Spatial distribution of heating rates in the ANL-TEPR inner shield.

reference design have a chance of reaching the low-energy range compared with 90% in a mostly lithium blanket.

Figure 15 shows a maximum nuclear-heating rate of ~2.1 W/cm^3 for a neutron wall loading, W_n, of 0.2 MW/m^2 in the first wall. The nuclear heating drops by about an order of magnitude in the first 15 cm of stainless steel in the blanket, then rises again to 1.05 W/cm^3 in the inner part of the next boron-carbide zone. More than 60% of the heat generated in stainless steel comes from absorption of the secondary gamma rays. Energy deposition by neutron interactions dominates the nuclear heating in boron carbide, primarily because of the large (n,α) cross section in ^{10}B with a Q-value of +2.49 MeV. The nuclear heating rate per unit volume in boron carbide is a factor of ~3 higher than the neighboring stainless-steel regions. This is not expected to cause any severe difficulties in the design of the heat transfer system, since B_4C can be operated at much higher temperatures than stainless steel.

The total energy deposition in the shield, which starts at ~40 cm from the first wall, is only 1% of that in the blanket. The heat-generation rate per unit volume in the inner shield varies from a maximum of ~2×10^{-2} to a minimum of 1×10^{-5} W/cm^3. Although these rates may be too low to allow heat removal with a high thermodynamic efficiency, cooling of the shield is necessary to ensure its physical integrity.

Figure 17 shows the atomic displacement in stainless steel as a function of position in the blanket/shield in units of dpa for an integral wall loading of 1 (MW yr)/m^2. The spatial distributions of the hydrogen- and helium-production rates in stainless steel are shown in Fig. 18. In the first wall, the rate of atomic displacement is 11 dpa per (MW yr)/m^2 and the rates of helium and hydrogen production are 216 and 531 appm per

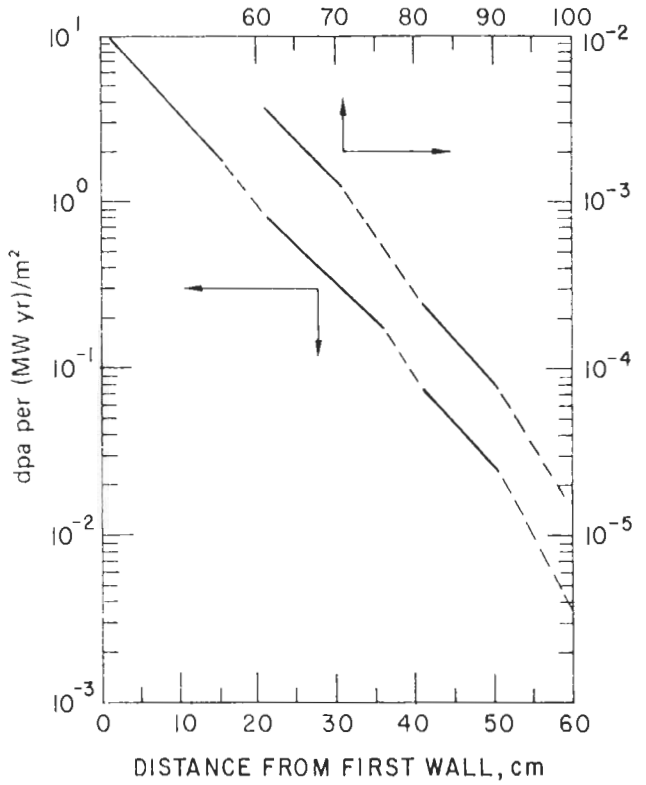

Fig. 17. Spatial distribution of atomic displacements in the stainless-steel regions of the ANL-TEPR blanket/shield for an integral neutron wall loading of 1 (MW yr)/m².

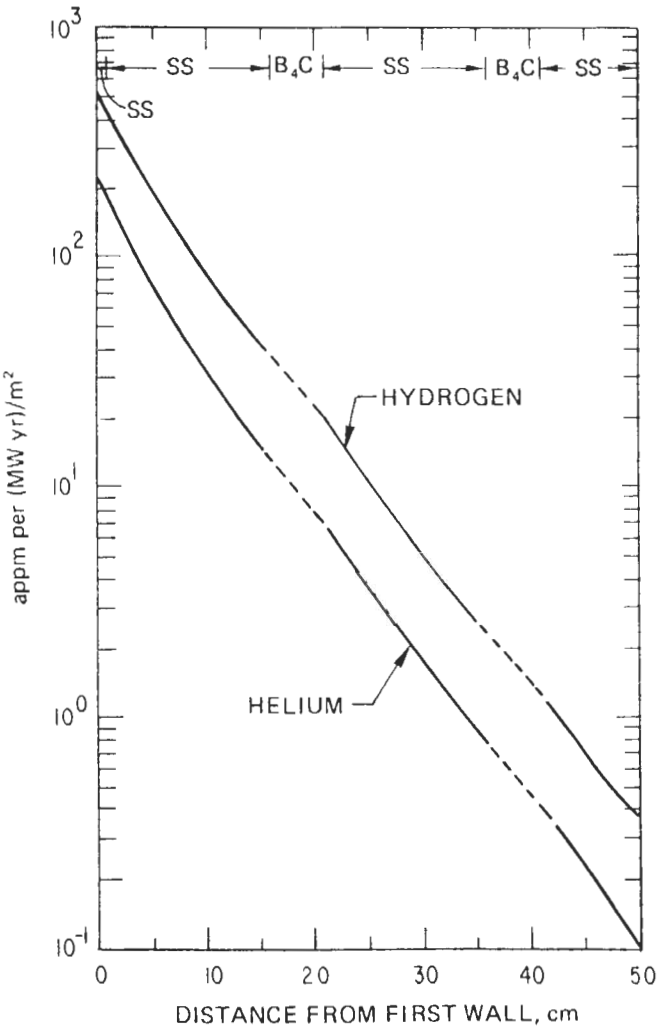

Fig. 18. Spatial distribution of hydrogen and helium production rates in the stainless-steel regions of the ANL-TEPR blanket [production rates given in atomic parts per million for an integral wall loading of 1 (MW yr)/m²].

(MW yr)/m². The first wall is expected to operate satisfactorily under these conditions for ~1 (MW yr)/m² based on radiation damage limits of 5% swelling and 1% ductility.[4] Therefore, the present design, with a neutron wall loading of 0.2 MW/m² could be expected to operate for approximately 10 yr with a duty factor as high as 50% before the replacement of the first wall becomes necessary. The gas-production rates drop by approximately an order of magnitude in the first 15 cm while the rate of atomic displacement decreases by only a factor of 6. Replacement of the 15-cm stainless-steel regions behind the first wall may be required for extended operation as a radiation test facility. Replacement of other stainless-steel zones inside the blanket is not likely to be necessary because of the large decrease in radiation damage-related parameters (gas production and dpa) and the fact that most of the stainless steel in the blanket does not serve any structural purposes.

Tritium contamination of the heat transfer system is an important concern in the TEPR design. Tritium can reach the coolant from two sources: (a) tritium diffusing from the plasma region through the first wall, and (b) tritium generated from neutron-induced reactions in the blanket/shield. In the Stage I-blanket/shield (no lithium) of the ANL-TEPR reference design, tritium is produced by the (n, t) reactions in ^{10}B and ^{11}B. For W_n = 0.2 MW/m² and 50% duty cycle, the amount of tritium generated by these reactions is ~10 g/yr. More than 90% of this tritium is produced in zone 5, which consists of 5 cm of boron carbide (see Tables VII and VIII). This amount of tritium is larger than that diffusing from the plasma region through the stainless-steel first wall but tritium diffusion in boron carbide is very slow if its operating temperature can be maintained reasonably low. However, if the level of tritium inventory in boron-carbide or the rate of tritium escape into the coolant are unacceptable, the boron-carbide in zone 5 can be replaced with

stainless steel. This will result in a slight improvement in the attenuation of nuclear radiation but will increase the level of induced radioactivity.

IV.B. Nuclear Heating and Radiation Damage in the Magnet

Figure 19 shows the spatial distribution of nuclear heating in the inner segment of the toroidal field magnet (i.e., along line A-D in Fig. 14) in units of W/cm^3 for a neutron wall loading of 0.2 MW/m^2. The maximum nuclear heating in the magnet conductor is 5×10^{-6} W/cm^3. Assuming the spacing between coolant channels is 10 cm, and using the physical properties of copper and Nb–20 Ti at 80 kG and 4.2 K, the maximum temperature rise inside the superconductor is only a few millidegrees Kelvin. Thus, the nuclear heating could be increased by two orders of magnitude and the spacing between coolant channels adjusted to limit the maximum temperature rise in the superconductor to 1 K without any practical difficulty. Note that the total heating rate in the magnet is the sum of the nuclear heating rate shown in Fig. 19 plus the contribution from thermal leakage.

The total nuclear-energy deposition in the magnet is 0.14 W/cm in the toroidal direction for a neutron wall loading of 0.2 MW/m^2. The ANL-TEPR has 16 magnets with a magnet width of 114 cm. Therefore, the total nuclear-energy deposition is 16 W per magnet and 256 W for all 16 magnets.

For the purpose of these calculations, the toroidal-field magnet was homogenized as 44% copper, 44% stainless steel, 6% niobium-titanium, and 6% helium. However, in the actual engineering design of the ANL-TEPR, the toroidal-field coil windings are separated from the shield by ~3 cm stainless-steel bobbin wall, ~3 cm vacuum space, and ~2 cm stainless-steel Dewar wall. In the following, conservative estimates of the maximum radiation damage values in the magnet conductors and insulators are calculated at a depth of 3 cm within the homogenized composition of the magnet.

Figure 20 shows the atomic displacement and the radiation-induced electrical resistivity, ρ_r, as a function of the copper stabilizer position in the magnet. The maximum ρ_r is 2.5×10^{-8} Ω-cm for an integral wall loading of 10 (MW yr)/m^2. A fully stabilized conductor designed to operate at 80 kG requires a 25% increase in the amount of copper stabilizer to compensate for this increase in the copper resistivity so that the total stability criterion is kept satisfied. This represents no

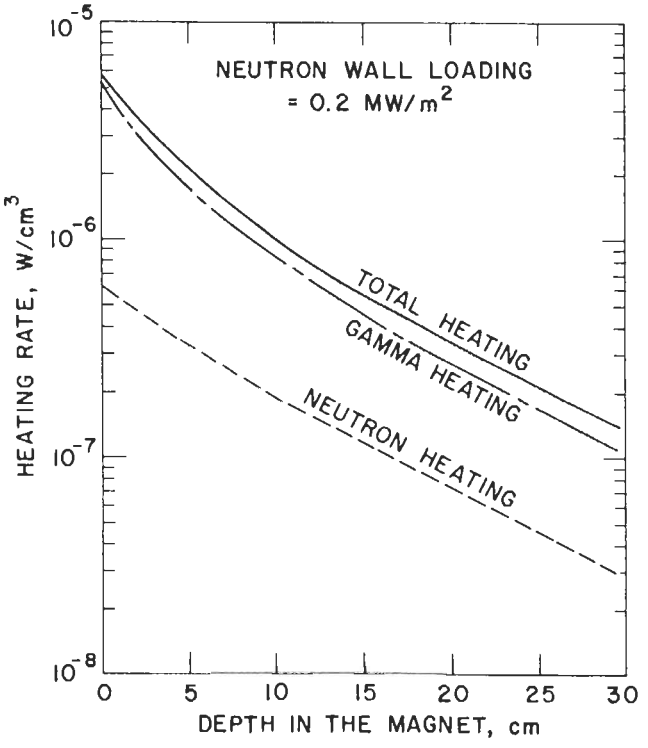

Fig. 19. Spatial distribution of heating rates in the inner segment of the ANL-TEPR toroidal field magnet.

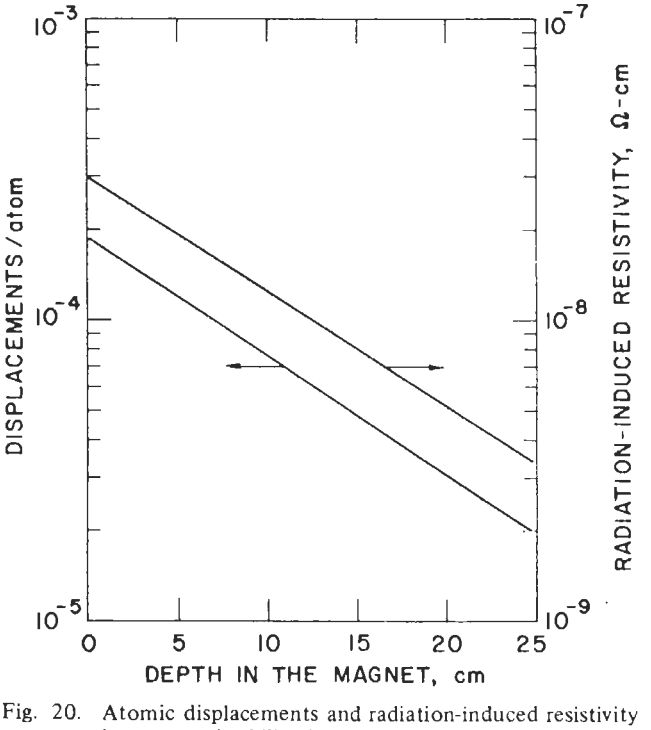

Fig. 20. Atomic displacements and radiation-induced resistivity in copper (stabilizer) as a function of depth within the inner segment of the toroidal field magnet after reactor operation for an integral wall loading of 10 (MW yr)/m^2.

serious difficulty in a practical conductor design. Since the useful working stress for copper at 4.2 K is about half that of stainless steel, the amount of the stainless-steel structure can be reduced by about half the increase in copper. The radiation-induced resistivity in copper decreases to a value of $\sim 5 \times 10^{-9}$ Ω-cm at a depth of 20 cm in the magnet; this requires less than a 5% increase in the amount of copper.

The TEPR is not expected to operate continuously for 10 (MW yr)/m^2 of integral neutron wall loading. In addition, the radiation-induced resistivity in copper can be recovered by annealing at elevated temperatures. Since it takes ~2 to 3 months to cool down the magnet from room temperature to 4.2 K, it is not desirable to warm up the magnet very frequently. However, there will certainly be down periods for maintenance, replacement of experimental blanket modules, etc. during which magnet warmup can be scheduled. The neutron wall loading for the ANL-TEPR design is calculated to be 0.2 MW/m^2. Due to a multiplicity of uncertainties in the plasma characteristics, the same design may be capable of producing much more (or less) power than expected. Furthermore, there is uncertainty in deriving radiation damage-related parameters in the magnet because of uncertainties in nuclear data and transport calculations, in addition to uncertainties in translating the neutronics parameters into radiation-damage effects. After the superconducting magnet is built, it will not be possible in many instances to modify it to accommodate any unexpected changes in the reactor performance. Therefore, it appears that a prudent design should allow a safety factor of 5 to 10 in neutronics parameters pertinent to the magnet design.

The important impurities produced by transmutations in copper are nickel, zinc, and cobalt. The maximum impurity concentration in the copper of the ANL-TEPR magnet is 0.003 appm per (MW yr)/m^2, most of which is ^{64}Ni, ^{64}Zn, and ^{66}Zn produced by radioactive decay of the products from radiative-capture reactions in ^{63}Cu and ^{65}Cu. This level of impurity concentration is a few orders of magnitude lower than that normally present in OFHC copper[35] commonly used as the stabilizer in superconducting magnets. Therefore, effects of impurity production in copper on the electrical resistivity do not present any problem in the ANL-TEPR design. Figures 21 and 22 show the spatial distribution of hydrogen and helium production rates, respectively, in appm per (MW yr)/m^2 in the copper stabilizer, in the NbTi superconductor, and in the stainless-steel structure of the magnet.

The ANL-TEPR magnet design uses Mylar as the thermal and electrical insulation in the toroidal-field coils. Figure 23 shows the absorbed dose from nuclear irradiation in Mylar as a function of its position inside the inner magnet. The maximum dose in Mylar is $\sim 4 \times 10^7$ rad for an integral neutron wall loading of 1 (MW yr)/m^2. Investigation of radiation effects in polymers in air indicates[36,37] that Mylar and epoxy can operate satisfactorily under room temperature irradiation for doses up to 1.2×10^8 and 3×10^9 rad, respectively. Thus Mylar can sustain damage in the ANL-TEPR magnet up to an integral wall loading of ~3 (MW yr)/m^2. For a wall loading of 0.2 MW/m^2, 50% duty cycle, Mylar insulation can perform its function properly for ~30 yr. It should be noted that replacement of interlayer insulation between the conductor and the structure is not practical. Therefore, the design value for the useful lifetime of the interlayer insulation should be about the same as that of the TEPR plant. Mylar appears adequate in this regard according to the present calculations. However, if radiation damage to the polymeric materials proves more serious at cyrogenic temperatures than that at room temperatures, Mylar will have

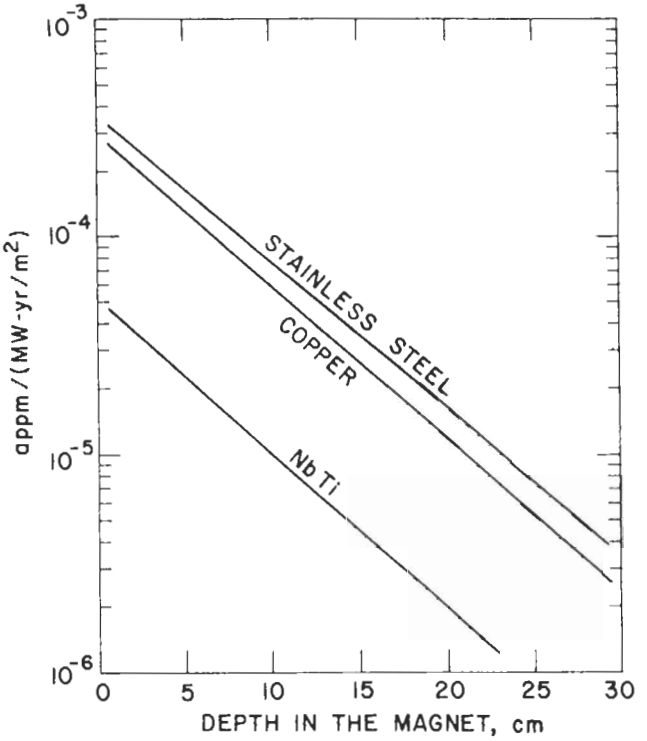

Fig. 21. Spatial distribution of hydrogen production rates [in atomic parts per million for integral wall loading of 1 (MW yr)/m^2] in structural material (stainless steel), superconductor (NbTi), and stabilizer (copper) as a function of depth in the inner segment of the toroidal field magnet.

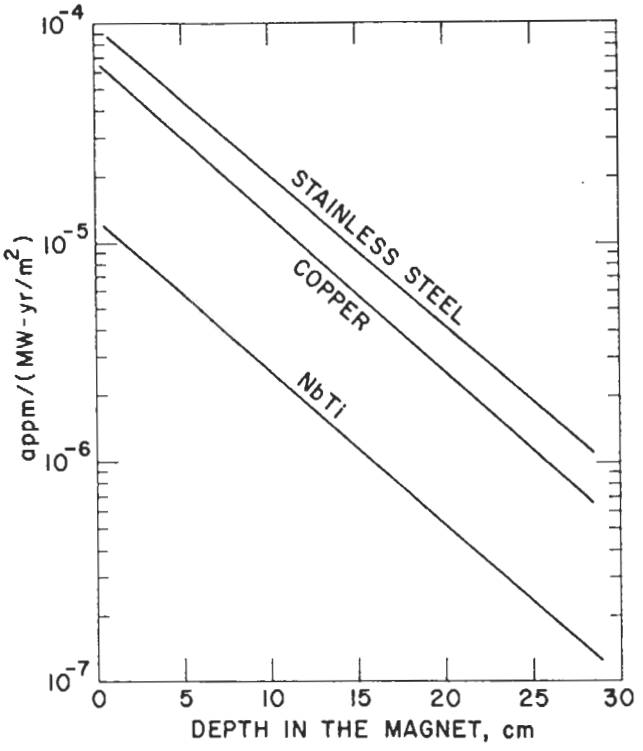

Fig. 22 Spatial distribution of helium production rates [in atomic parts per million for an integral wall loading of 1 (MW yr)/m²] in structural material (stainless steel), superconductor (NbTi), and stabilizer (copper) as function of depth in the inner segment of the toroidal field magnet.

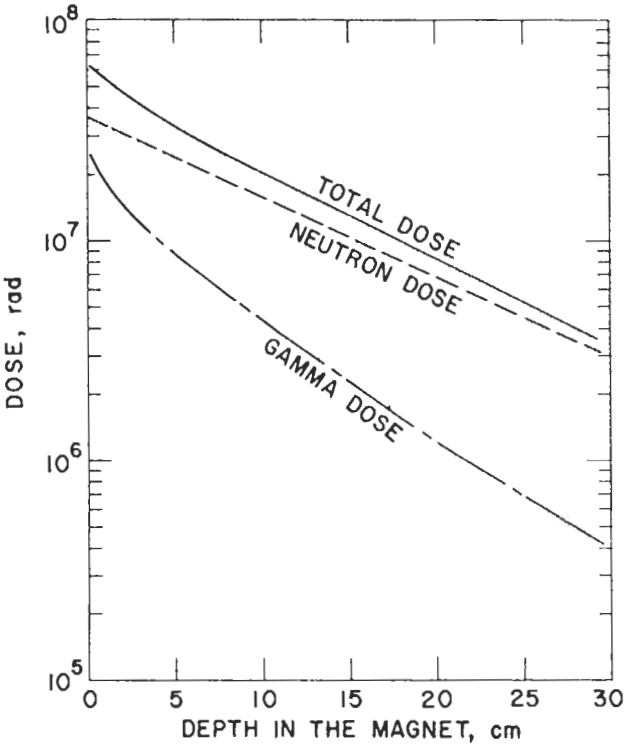

Fig. 23 Dose absorbed in Mylar as a function of Mylar position in the inner segment of the ANL-TEPR toroidal field magnet for an integral neutron wall loading of 1 (MW yr)/m².

to be replaced by other types of insulators, e.g., epoxy. The useful lifetime of epoxy is ~20 times longer than that of Mylar under the same irradiation conditions.

IV.C. Biological and Local Shielding

Because of cost and other considerations, the magnet shield is kept to the minimum size that satisfies the magnet protection criteria. This shield is not sufficient to reduce the biological dose to the level allowed for occupationally exposed individuals. Therefore, additional biological shielding, surrounding the walls of the reactor building, must be provided to reduce the biological dose during full power operation to ~1 mrem/h. The biological dose referred to here is based on Kerma[38] for tissue with the elemental composition of a STANDARD MAN (Ref. 39) and includes both neutron and gamma-ray contributions.

During operation of the ANL-TEPR reference design with a neutron wall loading of 0.2 MW/m², the biological dose at a location just outside the shield in the space between magnets (point E in Fig. 14) is 3×10^5 mrem/h. The biological dose at a location just outside the outer part of the magnet is 2×10^3 mrem/h. Thus the 57-cm magnet provides for only two orders of magnitude reduction in the biological dose. This reflects the fact that the magnet constituents (mainly copper and stainless steel) are not very effective in attenuating neutrons in the keV and low-MeV energy range, which constitute the largest component of the neutron spectrum in the magnet. Since most of the neutrons and gamma rays reaching the walls of the reactor building (inner part of the biological shield) come from the gap between magnets, ignoring the attenuation effects of the magnet provides a conservative basis for the design of the biological shield.

Since space has to be provided outside the magnet for necessary equipment, the neutron and gamma-ray fluxes at the inner surface of the biological shield will be lower than those at the magnet shield. Calculation of this geometry effect awaits more detailed information than is currently available for the reference design, but a crude estimate shows roughly a factor of 2 reduction in the fluxes. Ordinary portland concrete is relatively inexpensive, and a 97-cm-thick biological shield of concrete is sufficient to reduce the biological dose during full-power operation to

1 mrem/h. The maximum nuclear-heat-generation rate in the concrete is $\sim 10^{-7}$ W/cm^3, and no external cooling of the biological shield is required.

The engineering design for TEPR must allow for many penetrations such as those for beam injection, pumping, and diagnostics. The penetrations through the blanket, magnet shield, building walls, and biological shielding must be carefully investigated in the nuclear design analyses for TEPR. Adequate shielding must be provided to protect against streaming of nuclear radiation through these penetrations. Furthermore, some of the necessary equipment placed outside the torus are sensitive to nuclear radiation and need to be protected by providing local shielding. The treatment of shielding for penetrations and external equipment requires, in general, three-dimensional neutron and gamma-ray transport calculations and depends greatly on the details of the design investigated. This subject is not examined here as the present study deals with the general features of the blanket/shield design that are very likely to be common to all TEPR designs.

IV.D. Alternative Designs for the Inner Blanket/Shield

The concept of two separate segments for the blanket/shield system was introduced earlier in this section. One segment, called the inner blanket/shield, occupies the region of high-magnetic field, is constructed from very efficient attenuators, and its dimensions are determined only by the magnet protection criteria. The other segment, the outer blanket/shield, is constructed in the low magnetic-field region with materials and dimensions subject to all other constraints such as cost and induced activation, in addition to satisfying the magnet-protection criteria and reducing the overall power requirements of the cryogenic system. The purpose of this subsection is to examine in greater detail the merits of the two-segment blanket/shield system and to investigate alternative materials for the inner blanket/shield.

Results in Sec. II show that a SS-B_4C mixture is superior, in terms of attenuation, to all other material compositions investigated except for W-B_4C and Ta-B_4C mixtures. At current prices, the cost per unit volume of tungsten and tantalum is roughly two orders of magnitude higher than that for any other material considered in this study. Constructing the entire blanket/shield system from tantalum or tungsten can be easily rejected on the basis of the very high cost involved. However, the use of tungsten or tantalum in the relatively small volume of the inner blanket/shield can be very advantageous.

Table X gives a description of four alternative designs for the inner blanket/shield. Design I is the reference design discussed in the previous subsections and consists of alternating zones of stainless steel and boron carbide with a total blanket/shield thickness, Δ_{BS}, of 100 cm. Design II is the same as Design I except stainless steel is replaced by tungsten in zones 4, 6, and 10. Design III uses tungsten and boron carbide as Design II does but with a near-optimal arrangement of tungsten and B_4C. Design IV was obtained from Design III by replacing tungsten with tantalum

TABLE X

Description of Alternative Designs for the Inner Blanket/Shield System

Zone	Radial Position (cm)	Thickness (cm)	Density Factor	Design I[a]	Design II	Design III	Design IV
1	0–210	210	0	Plasma	Plasma	Plasma	Plasma
2	210–240	30	0	Vacuum	Vacuum	Vacuum	Vacuum
3	240–241	1	0.5	SS	SS	SS	SS
4	241–256	15	0.9	SS	W[b]	W	Ta[c]
5	256–261	5	0.9	B_4C	B_4C	W	Ta
6	261–276	15	0.9	SS	W	W	Ta
7	276–281	5	0.9	B_4C	B_4C	B_4C	B_4C
8	281–291	10	0.95	SS	SS	SS	SS
9	291–301	10	0.95	B_4C	B_4C	W	Ta
10	301–311	10	0.95	SS	W	W	Ta
11	311–321	10	0.95	B_4C	B_4C	W	Ta
12	321–331	10	0.95	SS	SS	SS	SS
13	331–340	9	0.95	B_4C	B_4C	B_4C	B_4C
14	340–397	57	1	magnet (44% SS + 44% Cu + 6% NbTi + 6% He)			

[a] Reference design.
[b] Tungsten alloy.
[c] Tantalum alloy.

on a 1-to-1 volume basis. The pure metals tungsten and tantalum were used to approximate the easily fabricated nonmagnetic tungsten- and tantalum-base alloys. A reasonable amount of stainless steel was retained in all designs to satisfy structural requirements.

Table XI compares the maximum values of the important radiation-damage parameters in the toroidal-field coil for the four designs. The results show that replacing stainless steel by tungsten in 40% of the blanket/shield volume reduces the radiation damage in the magnet by a factor of ~5. Using the optimal arrangement of W-B_4C in Design III results in an order of magnitude reduction in radiation damage to the superconducting magnet components, compared with the SS-B_4C reference design. The radiation level at the magnet is a factor of 6 lower for the Ta-B_4C design (Design IV) compared with the SS-B_4C design and ~60 higher than that for the W-B_4C design (Design III). Note that radiation attenuation for tungsten is better than that for tantalum on a volume basis, but the latter is better on material-weight basis.

The above results indicate clearly that, for a given level of radiation damage to the magnet components, Δ_{BS}, for the W-B_4C can be significantly less than that for the SS-B_4C blanket/shield. A blanket/shield of Design Type III with Δ_{BS} = 84.5 cm is equivalent in terms of magnet protection to the SS-B_4C reference design. Therefore, using W-B_4C in the inner blanket/shield allows the toroidal-field coils to be closer to the plasma. For the ANL-TEPR reference design, this results in 5.4% increase in the magnetic field at the plasma axis and ~24% increase in the reactor thermal power as well as a substantial improvement in plasma confinement.

The entire blanket/shield system is conceived to be constructed of several modules for many practical reasons, such as assembly, disassembly, and replacement. Therefore, constructing the inner blanket/shield module from materials different from those used in the modules of the outer blanket/shield should not involve any added difficulty or significant increase in the fabrication cost. However, use of tungsten or tantalum in the inner blanket/shield, instead of stainless steel, involves a cost penalty resulting from the large difference in material cost. This increase in cost depends greatly on the size of the inner blanket/shield. With the geometry parameters in Fig. 14, replacing the 100-cm SS-B_4C with the 84.5-cm W-B_4C increases the cost by ~34 million dollars on the basis of material cost of 2, 3, and 70 $/kg for SS, B_4C, and tungsten, respectively. (Note that the average major radius for the inner blanket/shield is only 335 cm.) This cost is directly proportional to the angle, θ, formed by the boundaries of the inner blanket/shield at the plasma centerline (θ = 50 deg in Fig. 14). The angle θ must be large enough to reduce the overall power requirements of the refrigerators and small enough to limit the amount of tungsten used. In the present design, θ can be reduced to 30 deg without increasing the power required to run the refrigerators beyond 1% of the plant electrical power output. The added capital cost of 20 million dollars in this case could probably be justified on the basis of the 24% increase in the reactor power output and the substantial improvement in confinement.

V. SUMMARY AND CONCLUSIONS

A TEPR that produces tens of megawatts of electrical power and has most subsystems prototypical of the demonstration power plant is planned[3] as the next step beyond the Tokamak Fusion Test Reactor.[2] Important considerations in the nuclear design of the blanket/shield system were investigated for a TEPR that operates on the D-T cycle and uses superconducting toroidal field coils. The reactor size and cost for a specified power output are very sensitive to the blanket/shield dimensions, particularly when NbTi, in which the maximum practical magnetic field is limited to ~80 kG, is used as the superconductor.

The nuclear performance of various blanket/shield material compositions was studied. It was

TABLE XI

Effects of Using Tungsten and Tantalum Alloys in the Inner Blanket/Shield of the Reference Design

Maximum Values in the Inner Magnet[a]	Design I	Design II	Design III	Design IV
Displacements in copper, dpa per (MW yr)/m^2	1.5×10^{-5}	3.0×10^{-6}	1.4×10^{-6}	2.3×10^{-6}
Radiation-induced resistivity in copper, Ω-cm for 10 (MW yr)/m^2	2.5×10^{-8}	5.0×10^{-9}	2.4×10^{-9}	3.9×10^{-9}
Neutron fluence, n/cm^2 per (MW yr)/m^2	4.7×10^{16}	9.3×10^{15}	1.2×10^{16}	1.5×10^{16}
Dose in Mylar, rad per (MW yr)/m^2	3.7×10^{7}	7.4×10^{6}	4.0×10^{6}	6.2×10^{6}

[a] Calculated at a depth of 3 cm within the homogenized composition of the magnet.

shown that in terms of nuclear radiation attenuation, stainless steel-boron carbide is superior to all other compositions investigated except for tungsten-boron carbide and tantalum-boron carbide mixtures. The optimum composition for a stainless steel-boron carbide (B_4C) mixture is 50 vol% SS + 50 vol% B_4C for minimum atomic displacement in the magnet copper stabilizer and 75 vol% SS + 25 vol% B_4C for minimum energy deposition in the toroidal field coils. Using helium coolant increases the blanket/shield thickness by a few percent as compared to water cooling. The use of graphite and aluminum in the TEPR blanket/shield is desirable from the viewpoint of low induced activation and easing the requirements on the remote handling system. However, these materials are not very effective in attenuating neutrons and gamma rays and their use will involve a severe penalty in terms of increasing the blanket/shield thickness required to protect the superconducting magnet.

Results of irradiation experiments at liquid-helium temperatures on superconducting materials and normal metals were reviewed. Correlation between the radiation-induced electrical resistivity in copper and the number of atomic displacements was derived. It is generally accepted that the superconducting toroidal field coils for TEPR must be cyrogenically stable. Therefore, the increase in the electrical resistivity of the stabilizing metal must be carefully considered in the designs for the blanket/shield and magnet systems. Substantial recovery from radiation damage to the superconductor and stabilizer can be accomplished by room temperature annealing. This makes the magnet protection criteria closely related to many of the reactor design features such as the neutron wall loading, duty cycle, and the frequency that the magnet can be scheduled for warm up. No substantial recovery can be accomplished for radiation damage to the magnet insulators, and they should be sufficiently protected from nuclear radiation so that they function properly for the magnet lifetime. Depending on many of the reactor design parameters, the electrical power required to run the refrigerators of the toroidal field coils can be more limiting on the design of the blanket/shield than the magnet protection criteria.

A detailed description of the blanket and shield system for a reference TEPR design, ANL-TEPR (Ref. 4), based on the considerations of this study was presented. The ANL-TEPR is designed to operate in two stages. Stage I is devoted to verification of plasma characteristics and demonstration of power production capability. The blanket in this stage contains no lithium. The second stage will experiment with other aspects of a full-scale Tokamak reactor such as tritium production and extraction.

The severe restrictions on space in TEPR are greatly eased by a new concept of two separate segments of the blanket/shield. The inner blanket/shield occupies the region of high magnetic field, uses very efficient attenuators, and its dimensions are determined only by the magnet protection criteria. The outer blanket/shield is constructed with materials and dimensions subject to all other constraints (e.g., cost, induced activation, overall power requirements of the cryogenic system) in addition to the magnet protection criteria.

In the reference design for Stage I, the blanket/shield consists of an optimized composition of stainless steel and boron carbide (B_4C) with Δ_{BS} of 100 cm in the inner region and 131 cm in the outer region. The neutron wall loading, W_n, is 0.2 MW/m^2. The recoverable energy is ~17 MeV per fusion reaction. The nuclear heat generation rate varies from 2.1 W/cm^3 in the first wall to 10^{-5} W/cm^3 in the shield. In the stainless-steel first wall, the rate of atomic displacement is 11 dpa per (MW yr)/m^2 and the rates of helium and hydrogen production are 216 and 531 appm per (MW yr)/m^2. The first wall is expected to operate satisfactorily under these conditions for ~1 (MW yr)/m^2.

The maximum nuclear heating in the toroidal field coils is 5×10^{-6} W/cm^3; the resulting temperature rise in the superconductor composite is only a few millidegrees Kelvin. The total nuclear heating in the 16 magnets is 256 W. The maximum displacement rate in the copper stabilizer is 1.5×10^{-5} dpa per (MW yr)/m^2. The magnet is designed to accommodate a ρ_r of 2.5×10^{-8} Ω-cm in the stabilizer. For a 50% duty cycle, W_n, of 0.2 MW/m^2, and a safety factor of 10, the toroidal field coils can operate up to 10 yr before this value of ρ_r is reached and annealing becomes necessary. The maximum neutron fluence in the toroidal field coils is 4.7×10^{16} n/cm^2 per (MW yr)/m^2, and the corresponding change in the critical current density of the NbTi superconductor is small. The maximum dose in the Mylar insulation is 4×10^7 rad per (MW yr)/m^2; satisfactory operation up to 3 (MW yr)/m^2 is expected.

The concept and consequences of the two-segment blanket/shield system and alternative materials for the inner and outer regions were investigated in detail. It was found that replacing stainless steel in the inner blanket/shield by tungsten or tantalum alloy reduces Δ_{BS} by ~15%, which results in a 24% increase in the reactor thermal power as well as a substantial improvement in plasma confinement at an added material cost of ~34 million dollars.

ACKNOWLEDGMENTS

The author thanks W. M. Stacey, Jr., H. Henryson, II, V. A. Maroni, D. L. Smith, J. Jung, T. H. Blewitt, and B. S. Brown of Argonne National Laboratory for informative discussions and encouragement.

This research was supported by the U.S. Energy Research and Development Administration.

REFERENCES

1. S. O. DEAN et al., "Status and Objectives of Tokamak Systems for Fusion Research," WASH-1295, U.S. Atomic Energy Commission (1974).

2. "Two Component Torus-Joint Conceptual Design Study," Princeton Plasma Physics Laboratory and Westinghouse Electric Corporation (1974).

3. S. O. DEAN, "The Tokamak Fusion Reactor Research and Development Plan," *Trans. Am. Nucl. Soc.*, **21**, 14 (1975).

4. W. M. STACEY et al., "Tokamak Experimental Power Reactor Studies," ANL/CTR-75-2, Argonne National Laboratory (1975).

5. W. M. STACEY, Jr. and P. J. BERTONCINI, "Plasma and Reactor Parameters for a 150-MWth Tokamak Experimental Power Reactor Calculated on the Basis of Trapped-Ion-Mode Confinement Theory," *IEEE Conf. Records - Abstracts, The Second Int. Conf. Plasma Science*, May14-16, 1975, Ann Arbor, 75CH0987-NP5 (1975).

6. M. A. ABDOU, "Nuclear Design of Blanket and Shield for a Tokamak Experimental Power Reactor," *Trans. Am. Nucl. Soc.*, **21**, 27 (1975).

7. C. C. BAKER, "Design Considerations for Power-Producing Tokamak Devices with Noncircular Plasma Cross Sections," *Trans. Am. Nucl. Soc.*, **19**, 2 (1974).

8. P. H. SAGER, Jr., M. JONZEN, D. KEARNEY, R. THOMAS, W. TOFFOLO, and T. WOODS, "Conceptual Engineering Design Studies of a Fusion Experimental Power Reactor," *Trans. Am. Nucl. Soc.*, **21**, 25 (1975).

9. P. N. HAUBENREICH, D. G. McALEES, and M. ROBERTS, "The Tokamak Experimental Power Reactor; Scoping Studies," *Trans. Am. Nucl. Soc.*, **21**, 41 (1975).

10. P. N. HAUBENREICH, Ed., "Tokamak Experimental Power Reactor: Basic Considerations and Initiation of Studies at Oak Ridge," ORNL-TM-4853, Oak Ridge National Laboratory (1975).

11. J. T. KRIESE and D. STEINER, "Magnet Shield Design for Fusion Reactors," ORNL-TM-4256, Oak Ridge National Laboratory (1973).

12. M. A. ABDOU and C. W. MAYNARD, "Nuclear Design of the Magnet Shield for Fusion Reactors," *Proc. First Topl. Mtg. Technology of Controlled Nuclear Fusion*, CONF-740402-P1, Vol. I, p. 685, U.S. Atomic Energy Commission (1974).

13. T. A. GABRIEL, R. T. SANTORO, and W. W. ENGLE, Jr., "Shielding Design Calculations for ORMAK-F/BX," ORNL-TM-4619, Oak Ridge National Laboratory (1974).

14. W. W. ENGLE, Jr., "A User's Manual for ANISN," K-1693, Oak Ridge Gaseous Diffusion Plant (1967).

15. R. Q. WRIGHT et al., "SUPERTOG: A Program to Generate Fine-Group Constants and P_n Scattering Matrices from ENDF/B," ORNL-TM-2679, Oak Ridge National Laboratory (1969).

16. J. R. KNIGHT and F. R. MYNATT, "MUG: A Program for Generating Multigroup Photon Cross Sections," CTC-14, Oak Ridge Computer Technology Center (1970).

17. N. M. GREENE et al., "AMPX: A Modular Code System for Generating Coupled Multigroup Neutron-Gamma Libraries from ENDF/B," ORNL-TM-3706, Oak Ridge National Laboratory (1975).

18. M. A. ABDOU, C. W. MAYNARD, and R. Q. WRIGHT, "MACK: A Computer Program to Calculate Neutron Energy Release Parameters (Fluence-to-Kerma Factors) and Multigroup Neutron Reaction Cross Sections from Nuclear Data in ENDF Format," UWFDM-37, University of Wisconsin, and ORNL-TM-3994, Oak Ridge National Laboratory (1973).

19. M. K. DRAKE, Ed., "Data Formats and Procedures for the ENDF Neutron Cross Section Library," BNL-50279, Brookhaven National Laboratory (1970).

20. G. L. KULCINSKI, D. DORAN, and M. A. ABDOU, "Comparison of Displacement and Gas Production Rates in Current Fission and Future Fusion Reactors," *Proc. Seventh ASTM Int. Symp. Effects of Radiation and Structural Materials* (1974).

21. M. A. ABDOU, L. J. WITTENBERG, and C. W. MAYNARD, "A Fusion Design Study of Nonmobile Blankets with Low Lithium and Tritium Inventories," *Nucl. Technol.*, **26**, 400 (1975).

22. J. W. DAVIS, McDonnell Douglas Astronautics Company, Private Communication (1975).

23. R. A. KURTZ, "Properties and Design Considerations of High Density Metals," Technical Paper No. 634, Kulite Tungsten Corporation, Ridgefield, New Jersey (1967).

24. J. A. HORAK and T. H. BLEWITT, "Fast Neutron Irradiation Induced Resistivity in Metals," *Phys. Stat. Sol.*, **9**, 721 (1972).

25. M. SOELL, "The Influence of Low Temperature Neutron Irradiation on the Properties of Hard Superconductors," *Proc. 8th Symp. Fusion Technology*, Jutphaas, Netherlands (1974).

26. J. A. HORAK and T. H. BLEWITT, "Isochronal Recovery of Fast Neutron Irradiated Metals," *J. Nucl. Mater.*, **49**, 161 (1973); Errata, **50**, 315 (1974).

27. B. S. BROWN et al., "Low-Temperature Fast-Neutron Radiation Damage Studies in Superconducting Materials," *J. Nucl. Mater.*, **52**, 215 (1974).

28. M. SOELL et al., "The Influence of Low Temperature Neutron Irradiation on Superconducting Magnet Systems for Fusion Reactors," *Proc. 1974 Applied Superconductivity Conference* (Oct. 1974).

29. J. E. C. WILLIAMS, *Superconductivity and Its Applications*, Pion Limited, London (1970).

30. B. S. BROWN and T. H. BLEWITT, Argonne National Laboratory, Private Communication (1975).

31. J. PURCELL and S-T. WANG, Argonne National Laboratory, Private Communication (1975).

32. D. W. DeMICHELE and J. B. DARBY, Jr., "An Analysis of the Materials Constraints on Superconducting Magnets for Controlled Thermonuclear Reactors," *Proc. Symp. Technology of Controlled Thermonuclear Fusion Experiments and the Engineering Aspects of Fusion Reactors,* CONF-721111, p. 384, U.S. Atomic Energy Commission (1974).

33. D. W. DeMICHELE and J. B. DARBY, Jr., "A Summary of the Physics and Material Contraints on the Performance of Toroidal Magnets for Controlled Thermonuclear Reactors," *Proc. First Topl. Mtg. Technology of Controlled Nuclear Fusion,* CONF-740402-P2, Vol. II, p. 462, U.S. Atomic Energy Commission (1974).

34. M. A. ABDOU and C. W. MAYNARD, "Calculational Methods for Nuclear Heating–Part II: Applications to Fusion-Reactor Blankets and Shields," *Nucl. Sci. Eng.*, **56**, 381 (1975).

35. "Handbook on Materials for Superconducting Machinery," MCIC-HB-04, Metals and Ceramics Information Center, Battelle Columbus Laboratories (1974).

36. H. BRECHNA, "Effect of Nuclear Radiation on Organic Materials; Specifically Magnet Insulators in High Energy Accelerators," SLAC No. 40, Stanford Linear Accelerator Center (1965).

37. B. BADGER et al., "UWMAK-I, A Wisconsin Toroidal Fusion Reactor Design," FDM-68, University of Wisconsin (1973).

38. M. A. ABDOU and C. W. MAYNARD, "Calculational Methods for Nuclear Heating–Part I: Theoretical and Computational Algorithms," *Nucl. Sci. Eng.*, **56**, 360 (1975).

39. R. L. BACH and R. S. CASWELL, "Energy Transfer to Matter by Neutrons," *Radiation Res.*, **35**, 1 (1968).